Introduction to Metamaterials and Nanophotonics

Constantin Simovski and Sergei Tretyakov

Department of Electronics and Nanoengineering
School of Electrical Engineering
Aalto University
Finland

October 20, 2020

Contents

Chapter 10

Nanostructures for enhancement of solar cells

10.1 Introduction

The Sun is the main source of energy on Earth. The mankind has created passive and *active* technologies in order to use this energy. Active solar technologies are those which convert the sunlight energy into other forms. One of the most important active solar technologies is *solar photovoltaics*. Photovoltaic devices convert the electromagnetic energy of sunlight into electricity. The mechanism of this conversion is the *photovoltaic effect*. This effect is a special case of the so-called *photoelectric effect*, also called photoelectricity and photoinduction. Photoelectric effect is generation (induction) of conductivity charges in a semiconducting or conductive medium by absorption of incident light. The absorbed light increases the concentration of free charge carriers compared to the dark state of the same medium. In a semiconductor, photoelectricity is absorption of a photon resulting in excitation of an electron-hole pair. An electron transits to the conduction band, and in the valence band a hole appears. In other words, photoelectricity in a semiconductor is the same as optical excitation.

Photovoltaic (PV) effect is creation of voltage and electric current due to spatial separation of the photoelectric (photoinduced, photogenerated) charges. The *charge separation* prevents otherwise inevitable *recombination* of these charges. Charge separation is granted by an intrinsic electrostatic field that can exist in the illuminated medium. Separation of the photoin-

duced charges by the intrinsic field creates voltage (electromotive force) at the electrodes connected to the device. If an illuminated sample of the PV medium with an intrinsic field is connected to an external circuit, the positive and negative photoinduced charges (moving in the opposite directions) create *photocurrent*. This mechanism of light-to-electricity conversion is potentially the most efficient one [1].

10.1.1 A bit of history

In the year 1839, Edmond Becquerel (father of Henri Becquerel who discovered radioactivity), was a student and experimented in the laboratory of his father, Antoine-César Becquerel, who was a pioneer of a new science called *electrochemistry*. Edmond illuminated a circuit comprising a silver halide electrode submerged into an electrolyte by a collimated light beam. The illumination changed the current in the circuit. Then the battery was disconnected from the circuit. However, some short-circuit current arose when the light beam illuminated the contact [2]. It was historically the first *PV cell*, though not efficient enough for practical generation of electricity. In 1879, W. Adams and R. Day studying the PV effect in different media substituting silver halide revealed for *gray selenium* much higher photocurrent than that observed in all previous studies [3]. In 1883, Charles Fritts found that infrared light does not produce photocurrent in these elements, that electrolyte is not necessary, and that the best illumination is normal to the surface of the gray selenium layer. He achieved for a PV cell impinged by collimated solar light an unprecedented *overall efficiency* about 1%. Overall efficiency is the ratio of the electric power delivered in the external circuit to the light power incident on the cell. This ratio depends on the loading resistance – maximal power is delivered to the load whose resistance equals to that of the cell. The overall efficiency is the ratio of this maximal output power to the power of the incident light.

The PV cell suggested by Fritts as a source of electricity was implemented as a millimetre-thick gray selenium layer on a platinum substrate whose top surface was covered by a strongly submicron (partially penetrable for light) gilding [4][1]. The work by Fritts allowed scientists to understand that the PV effect is frequency-selective and to assume that the photocurrent

---

[1]Modern estimates have shown that the golden film in this experiment was 40–60 nm thick.

arises in the bulk of gray selenium and not only in the contact area. In 1888, Aleksander Stoletov (Stoletow) proved the direct proportionality of the photocurrent in this PV cell to the absorption of the visible light in the layer of gray selenium [5]. It was understood that the absorbed light converts into electricity namely in the semiconductor. All these studies were only prerequisites for the breakthrough in photovoltaics done by Albert Einstein. In work [6] Einstein explained both photoelectricity and its implication – PV effect. His explanation paved the road to really efficient PV cells – gave birth to solar photovoltaics. For this theory Einstein was awarded by his second Nobel prize (1921).

10.1.2 On enhancement of solar cells by passive nanostructures

Solar cells (SCs) are PV cells whose excitation is done by the Sun. Sunlight has a very broad frequency spectrum. On the Earth surface the main part of the direct sunlight spectrum comprising nearly 90% of the whole power covers a part of the near infrared range (770–900 nm) and the whole visible range (λ =400–770 nm). 10% of the power refer to the UV tail (320–400 nm) and three infrared sub-bands (λ =950–1050 nm, 1100–1320 nm, and 1500–1800 nm) [7]. Though the operation band of practical SCs is more narrow that this consolidated ultra-broad band, an efficient SC is always a very broadband converter of light into electricity. This property determines the main difference of SCs from relatively narrow-band converters such as photodiodes used in sensing and other similar applications. Here, the main attention will be paid to nanostructures which enhance the operational characteristics of SCs. Nanostructures which we will discuss can be classified as *anti-reflecting coatings* (ARCs) or *light-trapping structures* (LTSs). The purpose of both of them is the same: to maximize the useful absorption of solar light, that is, absorption of sunlight converting into electricity inside the PV layer. Maximization of this absorption is the same as minimization of optical losses of a SC.

ARCs are used to minimize reflection loss. LTSs are used to minimize transmission through the device and parasitic scattering from the internal elements of the PV cell, which results in leakage of the light energy from the cell. In this chapter we explain how nanostructured ARCs and LTSs enhance the SC performance. However, in order to understand it one has to know

what needs to be enhanced. Therefore, a minimal insight into physics of a SC is necessary. Here we restrict the discussion by the most important class of SCs: solar photodiodes.

10.2 Basics of the diode solar cell physics

The following brief overview of operation of PV diodes and their main characteristics basically follows popular textbooks [7, 8]. Here we assume that the readers are familiar, at least in general, with the physics of a usual *semiconductor diode*.

10.2.1 Operation of a diode solar cell

The PV effect can be illustrated by the zone diagram of a p-n junction shown in Fig. 10.1 (left panel). This sketch also shows the energies of photons which are absorbed in the diode. Photons whose energy $\hbar\omega$ is lower than that of the semiconductor bandgap $W_g = \hbar\omega_g = W_c - W_v$ are absorbed without creating photoelectric charges, i.e. are lost (Loss 1). Photons whose energy $\hbar\omega$ exceeds that of the semiconductor bandgap $\hbar\omega_g$ generate electron-hole pairs in the material bulk. These charge carriers are born with some initial velocity (due to the pulse of the absorbed photon) and spatially separate, as it was pointed out by Einstein, before their recombination occurs. The lifetime of photoinduced charges in a semiconductor is much longer than the lifetime of the excited state in a fluorescent molecule of a dye. It can be sufficient to let these charges to pass though a rather thick layer of semiconductor. However, in the absence of intrinsic static field $\mathbf{E}$ inside the semiconductor volume, it is useless to illuminate the semiconductor sample. All photoinduced electrons and holes after their relaxation to the edge states of the valence and conductivity zones, respectively, will recombine.

If a static electric field $\mathbf{E}$ is present in bulk of a semiconductor, the generated electron and hole drift along $\mathbf{E}$ in the opposite directions. Then the photoelectricity is accompanied by the PV effect. For semiconductor PV materials the best way of getting the needed static field "for free" is building a diode. In the diode, static electric field is obviously present due to the junction of two parts of the sample which are doped differently. Recall, that at the contact of the p- and n-doped parts of a semiconductor, positive and negative charges form a bilayer called *depletion region* with some static
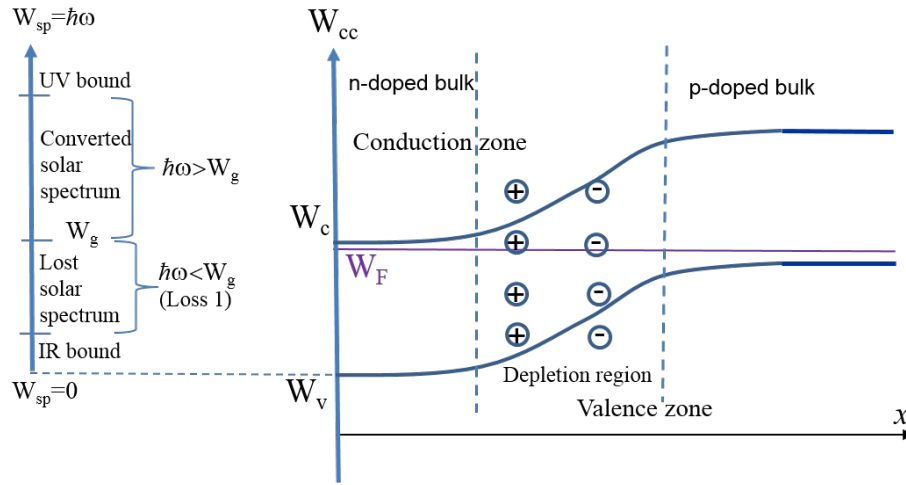
Figure 10.1: Left: Zone diagram of a dark semiconductor diode (no illumination). In this diagram, the energy of absorbed solar photons W_{sp} is shown for comparison with the energy levels W_v and W_c of the semiconductor. Subband solar light ($\hbar\omega < W_g = W_c - W_v$) is absorbed without producing the electron-hole pairs. Photons of higher frequencies are efficiently converted into electron-hole pairs. Right: Without light illumination, electrostatic field inside the depletion region of a semiconductor diode creates only the built-in voltage: No electromotive force is formed in the junction. The Fermi level W_F is uniform across the whole PV layer (this uniformity means the energy equilibrium of an unbiased junction).

electric field inside, like in a charged capacitor. The voltage V_c corresponding to this static field, called the *contact voltage* across the p-n junction, is close to the value of the semiconductor energy gap recalculated into a voltage $V_g = \hbar\omega_g/e$ ($e = -1.6 \cdot 10^{-19}$ C is the electron charge). This value in practice may attain $1 - 2$ V. The difference $V_g - V_c$ is relatively small and depends on the doping level.

The energy diagram of a p-n junction is shown in Fig. 10.1 together with the energy diagram of solar photons. The energy of absorbed photons is counted from the level W_c: the top edge of the conductivity zone of a semiconductor. In the absence of illumination, the *Fermi level W_F* is the same in both bulk p- and n-doped regions, meaning that if we connect the extremities of these regions with a wire, no current will flow. The diode is
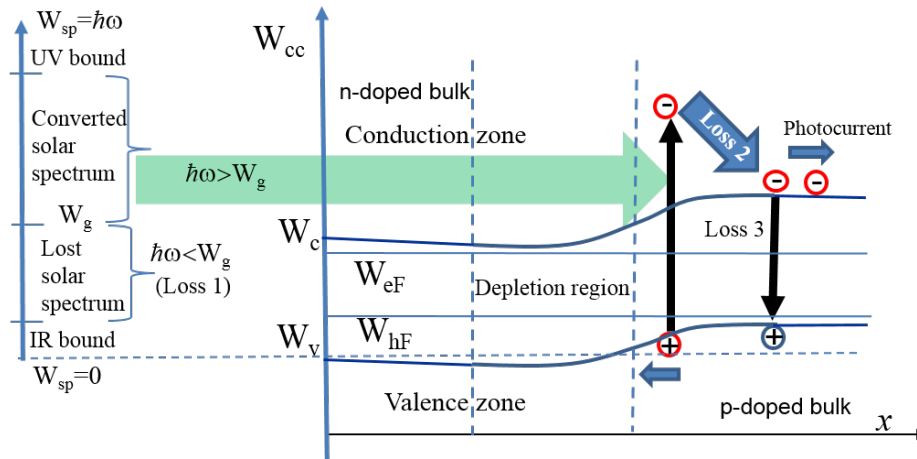
Figure 10.2: Zone diagram of an illuminated semiconductor diode and sketch of intrinsic losses of a SC. Illumination works as a direct biasing and destroys the uniformity of the Fermi level. Beyond the equilibrium one may introduce quasi-Fermi levels of electrons (W_{eF}) and holes (W_{hF}), uniform across the junction. Their difference determines the open-circuit voltage. Loss 1 is percentage of the sub-band sunlight. Losses 2 and 3 are illustrated for a photoinduced electron-hole pair in the p-doped region. A part of its energy $\hbar\omega - W_g$ is lost due to the relaxation process (Loss 2). Loss 3 is the probability of this pair to meet free charges of the opposite sign and to recombine. Losses 1–3 do not include the loss of useful photons ($\hbar\omega > W_g$) due to their possible reflection, scattering and absorption beyond the PV layer.

obviously not a power source and cannot discharge like a capacitor. In fact, the contact voltage is compensated by the outer voltages V_b created by weak electrostatic fields (of the opposite sign with respect to **E** in the depletion region). These fields exist in the bulk of the p-doped and n-doped parts called the quasi-neutral regions of the diode. As a result, the contact voltage is not an electromotive force and in the theory of p-n junction, V_c is called *built-in voltage*. So, in the dark regime there is no voltage between the extremities of the p-doped and n-doped regions of a diode.

Now imagine that the diode (prepared of a PV material) is illuminated by light. The processes in an illuminated diode are illustrated in Figs. 10.2 (zone diagram) and 10.3 (comparison of the *open-circuit* regime and *short-circuit* regime). The main absorption mechanism of useful photons ($\hbar\omega > \hbar\omega_g$) in a
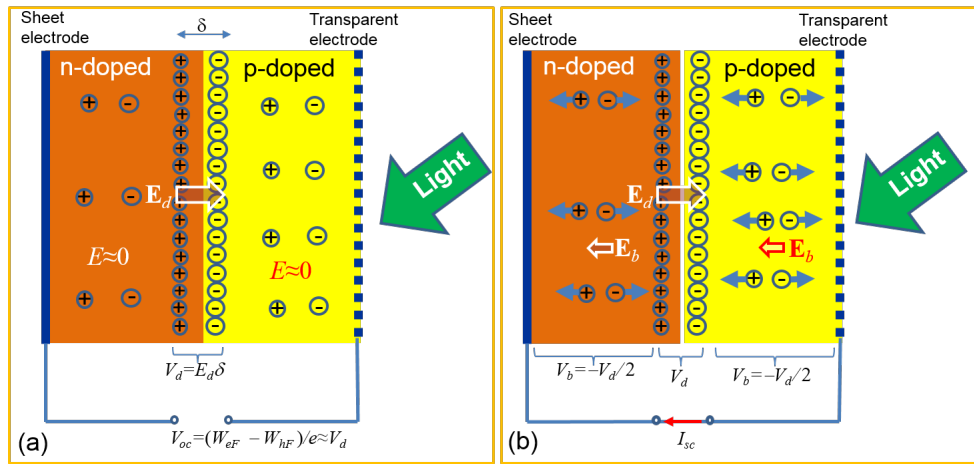
Figure 10.3: The static field in the bulk of a loaded photodiode results from the p-n junction. (a) Open-circuit voltage V_{oc} is practically equal to the voltage in the depletion region $V_d = E_d\delta$. No electric field in the bulk beyond the depletion region, no current flows, all photoinduced charges recombine. (b) In the short-circuit regime, voltage V_d cancels out with two voltages V_b applied to the bulk regions and corresponding to the field $\mathbf{E}_b$. This field urges the photocurrent to flow oppositely to the dark diode current.

PV material is generation of electron-hole pairs. These photoinduced charges break the equilibrium in the depletion region decreasing the electrostatic field in it, i.e. acting like a direct bias. They also break the equilibrium in the quasi-neutral regions and the Fermi level loses its physical meaning everywhere in the diode. Instead, one introduces the quasi-Fermi levels: that of electrons (W_{eF}) and that of holes (W_{hF}). Their difference implies an *open-circuit voltage* V_{oc} which arises across the diode.

Really, since the current cannot flow in the open-circuit diode, in the regime of steady illumination the left extremity (that of the n-doped region) turns out to be charged positively and the right extremity (that of the p-doped region) is charged negatively, as it is shown in Fig. 10.3(a). This way the built-in voltage in the illuminated regime extends between these extremities and transforms into the open-circuit voltage which is smaller than V_g but has the same order of magnitude. One can say that the illumination transforms the built-in voltage V_c into electromotive force V_{oc}. Photoinduced charges in the quasi-neutral regions screen the charges of the depletion region,

reducing the static field beyond it, and V_{oc} turns out to be close to $E_d\delta$ where E_d is the absolute value of the mean electrostatic field in the depletion region and δ is its thickness[2]. This situation is illustrated by Fig. 10.3(a).

Now let us connect the electrodes of our SC by a wire, as it is shown in Fig. 10.3(b). In this short-circuit regime, two drops of voltage V_b arise across the bulk n-doped and p-doped regions of the PV layer. These voltages compensate V_d, which is possible because the static field $\mathbf{E}_b \neq 0$ arises in the quasi-neutral regions (like it was in the dark regime). Again, this field is opposite to the built-in field of the depletion region. In this case, the current in the external circuit is maximal and equal to the photocurrent $I = I_{sc}$ (i.e. the *short-circuit current* and photocurrent are equivalent). From Fig. 10.3(b) it is clear that the photocurrent in both bulk regions is formed by the minority charge carriers: holes in the n-doped part and electrons in the p-doped part. This means that the photocurrent is directed oppositely to the usual diode current (called in the theory of solar cells the *dark current*).

10.2.2 About optimization of solar cells

In order to optimize the solar cell efficiency, one should minimize both the intrinsic losses and the optical loss resulting from absorption of sunlight beyond the *PV layer* and scattering to free space. This chapter mainly discusses reduction of the optical loss, which is attained in modern SCs with the use of nanostructures. These nanostructures are, however, not intrinsic parts of the PV layer. The main component of the SC is the PV layer and it must be designed separately. How to design it?

First of all, it must be performed of a *PV material* – a material which efficiently converts photons into electron-hole pairs. The percentage of useful photons producing photoinduced charges to the total amount of photons absorbed in the PV material is called *photoelectric quantum efficiency* or *photoelectric spectral response* of the material. PV materials suitable for solar photovoltaics are by definition materials for which this value is close to 100% at the maximum of the solar spectrum (green range) and weakly decreases with detuning so that to be significant in the whole useful part of the solar spectrum. However, this parameter for realistic materials is dispersive and its integral value (averaged over the useful spectrum) can be a value within

---

[2]In fact, quasi-Fermi levels W_{eF} and W_{hF} have no well-defined physical meaning in the quantum theory of a heterogeneous semiconductor. These values are used in the classical model through E_d and V_{oc}.

the interval 50–80% depending on the explicit PV material and on its doping level (if the doping level is reasonable, because in heavily doped materials photoelectric spectral response drops). Choosing among all semiconductors namely a PV material and optimizing its doping level we guarantee a rather high value of the integral photoelectric response.

Optimization of the PV layer implies the maximal possible reduction of intrinsic losses of a SC. The intrinsic power loss of a SC comprises losses of three types. Loss 1 – *sub-bandgap loss* – arises because the sunlight obviously comprises photons of energy $\hbar\omega < \hbar\omega_g = W_g$. The bandgap frequency ω_g of a PV semiconductor usually lies in the so-called inter-band range (wavelengths $\lambda =$770–1100 nm). The portion of the sunlight power in the long-wavelength part of the spectrum ($\lambda > 1100$ nm) is rather small (17%) and this power is most often sacrificed. For crystalline silicon, which is the most popular and one of the most efficient PV materials, $\lambda_g =$1050 nm, and the value of Loss 1 related to the PV cutoff at frequency $\omega_g = 2\pi c/\lambda_g$ is about 18%. Another reason for Loss 1 is a parasitic effect called the *Franz-Keldysh effect* [9, 10]. This is non-linear transfer of visible-light photons into IR range that takes place in semiconductors in presence of high static electric field **E**. We will see that such field is present in SCs and more or less significantly distorts the band structure. In obsolete SCs this static field was too high and the Franz-Keldysh effect increased Loss 1 quite noticeably. In modern SCs the Franz-Keldysh effect is very small. The value $\eta_{\mathrm{sp}} = (1 - \mathrm{Loss\,1})$ is called the *spectral efficiency* of the SC. For modern SCs based on c-Si $\eta_{\mathrm{sp}} \approx 81\%$.

The dissipative loss of the power for a given photon equals $\hbar\omega - \hbar\omega_g$ because the charge carriers obviously relax towards the edges of the bandgap before they attain the electrodes. The integral parameter describing the relaxation losses averaged over the whole useful spectrum is usually called Loss 2 or *super-bandgap loss*. Since Loss 2 is dissipative, it can be modelled as an additional resistance connected in series to that of Ohmic loss which arises due to the non-ideal photoelectric efficiency. The value of Loss 2 depends on the solar spectrum shape and the statistics of photogenerated charges in the PV material. Since the solar spectrum is ultra-broadband and its maximum on the surface of the Earth is in the green range, for practical PV materials a significant percentage of solar photons have the energy higher than $\hbar\omega_g$. It makes Loss 2 a large value: For practical SCs it is within the interval 30–60%. The explicit value of Loss 2 for a given material depends on several parameters: the doping level, the thickness of the PV layer, the geometry of the SC, etc. Notice, however, that the rather high value of Loss 2 (close

to 30%), inevitable for a simple or *single-junction SC* (the term "single-junction" also refers to *heterojunction* SCs such as modern silicon SCs). In a third-generation SC – in a monolithic *multijunction SC* and in a SC with parallel decomposition of the solar spectrum – solar spectrum is effectively split onto sufficiently narrow bands converted by different parts of the SC separately. In these advanced and very expensive SCs Loss 2 is reduced to 10-15%.

For single-junction SCs the problem of high Loss 2 is responsible for the inevitable choice of such PV materials which have noticeable Loss 1. The infrared part of the incident light power is sacrificed (in SCs based on crystalline Si, GaAs, Ge and other practical PV materials) and there is an optimum trade-off between Loss 1 and Loss 2. If we chose the bandgap frequency ω_g at the IR edge of the solar spectrum λ =1850 nm (this is the bandgap wavelength of InSe), we get rid of Loss 1 almost completely, but broaden the operational band of our SC so that 90% of solar photons have the energy higher than W_g. Then Loss 2 will increase nearly twice (from nearly 30% corresponding to SCs based on c-Si to nearly 60% corresponding to indium selenide SCs). Definitely, this increase will overcompensate the 18% gain in the spectral efficiency.

Thus, practical PV materials for solar photovoltaics are not only materials with high photoelectric spectral response in the solar spectral range. They are also materials whose ω_g is selected as a trade-off between Loss 1 and Loss 2. Notice, that Loss 2 for a given PV material can be somewhat reduced by the proper design of a SC. For obsolete silicon SCs with a simple p-n junction Loss $2 \approx 40 - 45\%$ [7]. For advanced silicon SCs Loss $2 = 30 - 35\%$ [12].

Loss 3 – *recombination loss* – is the percentage of photoinduced charges which recombine before they attain the electrodes. For our purposes it is enough to know that the recombination holds everywhere: at the surface illuminated by the sunlight, in the bulk of the semiconductor, in the depletion region of the p-n junction, and at the surfaces of the metal contacts). This effect is especially important for crystalline SCs with a thick PV layer for which the struggle against this effect drives advanced technical solutions.

The recombination in the bulk is reduced by the reduction of the PV layer thickness. Here it is worth to mention that the static electric field **E** in the bulk of PV layers with a thick depletion region is low because the modest contact voltage turns out to be applied to a thick layer. In this situation (that holds in the crystalline silicon SCs), the main mechanism of the separation of the photogenerated charges is their diffusion. Field **E** is needed only to ensure

the directional drift of the photogenerated charges towards the electrodes. Roughly speaking, the electric field makes the diffusion of charges directional. Since the mean speed of the carriers is mainly determined by diffusion, the effectively maximal path of the minority carrier in the PV layer (that of the electrons in the p-doped layer and that of the holes in the n-doped layer) is their diffusion length. It is a parameter of the PV material with a given level of doping. Thicknesses of the p-doped and n-doped sublayers of the PV layer should be smaller than the diffusion length. Otherwise, most of the generated charges recombine in the bulk before they attain the electrodes.

However, if these layers are thinner than the mean free path of the minority carrier such a PV diode will be also inefficient. Mean free path is of the same order as the thickness of the depletion region in a simple p-n junction. Very high strength of electric field in the depletion region of a thin p-n junction implies a rather low photoelectric quantum efficiency of this region. The light absorption in quasi-neutral regions is more efficient. One needs high light absorption in the depletion region for higher electromotive force (the open-circuit voltage) but this absorption holds with a low quantum efficiency and therefore results in a high Ohmic loss. Recall also that in the region of high electric fields the Franz-Keldysh effect further reduces the cell efficiency.

This dilemma has been resolved without a trade-off between Ohmic loss and electromotive force of the SC by replacement of simple p-n junctions by a heterojunction. Modern silicon SCs comprise a relatively thick weakly n-doped c-Si layer and a a heavily n-doped nanolayer on top of it. The bottom layer of the PV layer is p-doped. The main light absorption holds in the thick weakly doped layer because the thin n^+ layer on top is sufficiently transparent for the sunlight. The photoelectric quantum efficiency of the central layer is high because the electric field strength is not too strong. The light energy is effectively collected in this sublayer, since it plays the role of an effective depletion region, occupying most of the volume of the solar cell. Of course, the layer thickness is chosen so that not to exceed the diffusion length of the charge carriers, otherwise the recombination loss – Loss 3 – will be too high. Thus, the thickness of the region where the photocurrent is mainly generated is increased without damaging the quantum efficiency. For the optimal thickness of the PV layer chosen in this way (for c-Si its total thickness is of the order of 200 μm), the recombination of the photogenerated charges in the bulk is reasonably small and is within 5–10% [7, 8, 20]. The surface recombination in such SCs became the main issue since 1970s, when

heterojunction silicon SCs were created.

The surface of a crystal lattice is a kind of a crystal defect that results in appearance of defect states. These states called *surface states* arise inside the bandgap and their presence drastically enhances the probability of recombination. Therefore, the lifetime of the charge carriers generated near the open surface is reduced and they recombine fast. In modern SCs this problem is partially resolved using the so-called *chemical passivation* of the top surface – covering it with a material that eliminates surface states. It can be a dielectric whose lattice is compatible with that of the semiconductor. Alternatively, it can be a semiconductor with a large bandgap (e.g. with ω_g in the UV range) which weakly absorbs sunlight.

However, passivation resolves the issue of surface recombination only for the open surface of the PV layer. Recombination remains high on the interfaces between the optimally doped PV material and the metal of the contacts. The level of this surface recombination can be reduced preparing heavily doped areas near metal contacts. In this way, the contrast of two contacting materials is reduced, the transition of photoinduced charges across the interface is not drastically slowed, and they penetrate into metal before they would recombine. Thus, the heavily n-doped layer on top of c-Si SC serves not only for the formation of a heterojunction. It also grants reduction of surface recombination. As to the p-doped layer on the bottom, it modern silicon SCs it forms a p-p$^+$ junction with a heavily p-doped nanolayer. This layer grants reduction of surface recombination in the bottom part of the SC.

In the described layered design, the heavily n-doped layer is on the top, and parasitic absorption in it is tolerable, but not negligibly small. Moreover, the transparency of the top contact is granted by performing it as a wire mesh. We will discuss below why this mesh produces a significant shadow, so that a noticeable part of the PV layer is under the wires and stays always in the dark. Finally, the presence of metal strips on top of c-Si hinders its chemical passivation increasing the cost of this procedure.

Therefore, in more advanced silicon SCs both contacts are located at the bottom side of the PV layer. In this design, the two contacts usually form an interdigital structure of metal microstrips contacting with alternating heavily doped n- and p-regions on the bottom of the PV layer. Since these heavily doped regions are rather thin, only the recombination in the bulk of the PV layer is important. In this design, the intrinsic electric field (in multiple depletion regions) is not anymore vertical, and the paths of photoinduced carriers elongate. Therefore, the bulk recombination and Ohmic loss (Loss 2)

increases. However, this harm (about 10% for the overall efficiency) is over-compensated by gain in the optical efficiency and lower cost of passivation of the fully open top surface of these SCs [12], called *interdigital-back-contact* SCs .

To conclude this discussion, let us compare a semiconductor PV diode with the historically first SCs. These SCs were also PV diodes but they used the contact voltage at electrolyte-semiconductor (Becquerel) or metal-semiconductor (Fritts) interfaces. Such structures refer to the so-called *Schottky diodes*. SCs based on Schottky diodes are inefficient because the contact voltage is applied not to a quite substantial depletion region but to the sharp physical interface of two media. At this interface the intrinsic electric field is very high (theoretically singular for an abrupt junction) and the junction represents a potential barrier. The absolute majority of photogenerated charges are stuck on this barrier and are not separated before they recombine. Therefore, photocurrent in an illuminated Schottky PV diode is lower by an order of magnitude than that in a p-n diode or a heterojunction diode.

10.2.3   Volt-Ampere curve of a diode-type solar cell
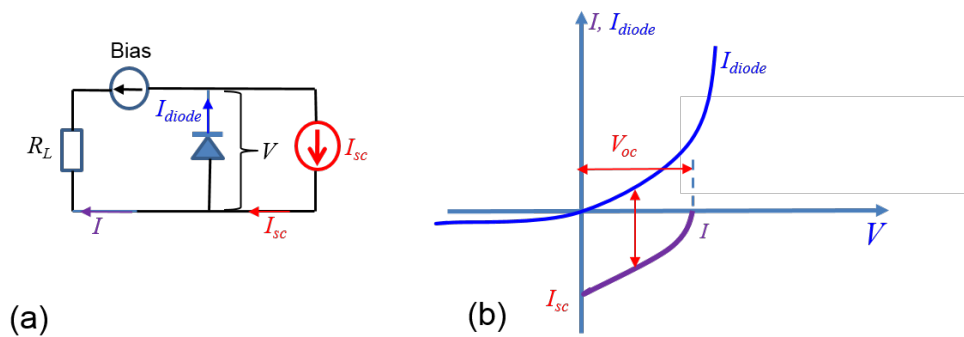
Figure 10.4: (a) Equivalent scheme of an illuminated and biased PV diode. (b) An *I-V* plot of the PV diode (blue curve) is obtained from the *I-V* plot of the same diode without illumination (magenta) by adding $-I_{sc}$ to I_{diode}. The solar-cell regime implies no external bias.

The usual operation regime of a PV diode is in the middle between two extreme regimes: the open-circuit one and the short-cut one. Let us briefly recall their definitions. If the external load resistance R_L is infinite, the

illumination of the diode results in the maximal possible drop of voltage between the electrodes, which is equal to V_{oc}, but the current is zero: All photogenerated pairs recombine in the same regions where they are born. In the short-circuit regime ($R_L = 0$), the current is maximal and equal to the photocurrent, whereas the drop of voltage is zero.

The maximal power in the external circuit corresponds to the matching condition when the load resistance equals to R_{iSC} of the illuminated SC. Since the photocurrent is the additive part of the diode current I and since it is directed oppositely to the dark current, the equivalent scheme of the loaded PV diode is a parallel connection of a current generator and a usual (not light-illuminated) diode, as shown in Fig. 10.4(a). An I-V dependency of an unbiased PV diode is represented by the bottom curve in Fig. 10.4(b). When $V > V_{oc}$ or $V < 0$, some external biasing is implied. However, it is not relevant for SCs. The Volt-Ampere curve of a SC corresponds to the case when the biasing is internal, that is, the bias is due the voltage drop across the load resistor R_L.

10.2.4   Main parameters of diode-type solar cells
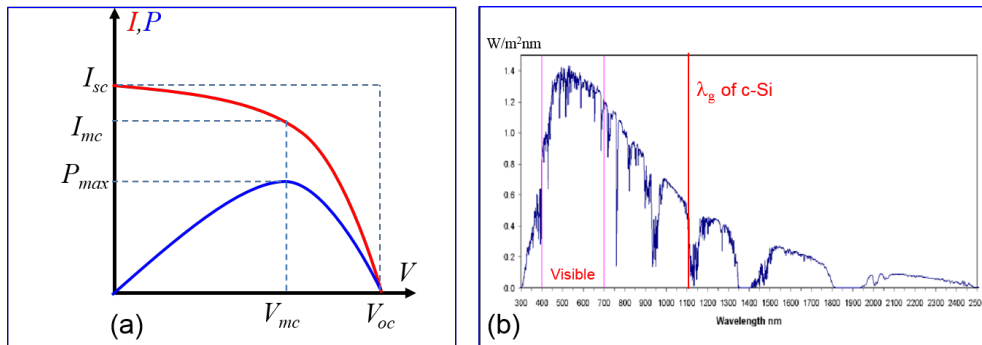
Figure 10.5: (a) I-V and P-V plots of a typical SC. Values I_{mc} and V_{mc} correspond to the matched regime when the delivered power attains its maximum $P_{\max}$. The fill factor is equal to $FF = I_{mc}V_{mc}/I_{sc}V_{oc}$. (b) Solar spectrum at the sea level. Loss 1 corresponds to the range $\lambda > \lambda_g$.

To discuss the main parameters of a SC it is instructive to consider such the I-V plot where the positive current direction is chosen so that I is positive. A typical I-V plot of a c-Si SC is shown in Fig. 10.5(a) together with the P-V

plot showing the output power versus V that practically implies variation of R_L. The maximal electric output $P_{\max}$ corresponds to the matched circuit (mc) regime. Corresponding values of the voltage and current are denoted as $V = V_{mc}$ and $I = I_{mc}$, respectively. The target is to maximally approach the *I-V* plot curve to a rectangle. Then $V_{mc} \to V_{oc}$ and $I_{mc} \to I_{sc}$. In this case, the value of $P_{\max}$ attains its absolute maximum $P_{\max}^{\max} = I_{sc}V_{oc}$, but it is achievable only theoretically. The ratio $P_{\max}/P_{\max}^{\max}$ for a realistic PV material is called the *fill factor* (FF). In some advanced SCs the fill factor is close to unity, e.g., for some cadmium telluride SCs $FF_{\max} = 0.93$ [12]. However, the most popular SCs for civil terrestrial applications are SCs based on c-Si. Panels of modern silicon SCs combine sufficient efficiency with reasonably low fabrication and exploitation costs and long life. Nowadays, their production does not imply any toxic waste. For silicon SCs the fill factor is in the interval $FF = 0.7 - 0.85$ depending on design specifics. This value enters the *overall efficiency of the SC* as a multiplicative factor.

Usually, in the analysis of the SC conversion efficiency one assumes that the bandgap of the semiconductor is chosen optimally as a compromise between Loss 1 and Loss 2, as explained above. In Fig. 10.5(b) the solar spectrum on the Earth surface is shown and the wavelength λ_g corresponding to the bandgap of c-Si is marked. Loss 1 is the area below the curve corresponding to $\lambda > \lambda_g$ divided by the area under the whole plot. Once the PV material is selected, this loss is determined. In calculations of the PV conversion efficiency, one considers the incident power as that of the useful solar spectrum – only the range $\lambda_{\min} < \lambda < \lambda_g$ is taken into account. Here $\lambda_{\min} = 320$ nm (937 THz) is the UV bound of the solar spectrum. Thus, the conversion efficiency of the SC is defined as the efficiency of conversion of the *useful power* of the sunlight into electricity in a system composed by a maximally illuminated SC and its matched load $R_L = R_{iSC}$.

Not all the incident power can convert into electricity due to many factors, such as non-ideal photoelectric quantum efficiency of the PV material, non-ideal fill factor, intrinsic losses of the PV layer and, finally, optical loss. Let us, first, define the optical loss (OL). It is the difference of the integral absorption coefficient A_{PV} of the PV layer from unity. A_{PV} is the integral of the time-harmonic absorption coefficient $A_{PV}(\lambda)$ over the band $\lambda_{\min} < \lambda < \lambda_g$ which takes into account the solar spectrum shape as a weight function. Since the number of photogenerated charge carriers is proportional to the number of absorbed photons, the conversion efficiency is directly proportional to A_{PV}. The latter is often called *optical efficiency of the SC*. Optical loss

$OL = 1 - A_{PV}$ is also called *matching loss*, because many researchers identify the optical loss with the reflection loss (the main loss factor for silicon SCs) and deduce the last one from the impedance mismatch of the illuminated surface and free space.

Intrinsic losses of the PV layer are called Losses 1, 2 and 3. Loss 1 has been discussed above. As to Losses 2 (relaxation loss) and 3 (recombination loss), they are taken into account calculating the so-called *internal quantum efficiency of the SC*. Above we have defined quantum efficiency of a PV material as a ratio of the number of electron-hole pairs induced in the PV material to the number of useful (above-bandgap) solar photons absorbed in the PV material during the same time. This quantum efficiency is a *photoelectric* parameter and sometimes is called *photoelectric spectral response*. Meanwhile, the internal quantum efficiency *of the SC* η_i is a PV parameter. By definition, it is equal to the ratio of the number of electron-hole pairs *reaching the electrodes of the SC* to the number of the absorbed useful photons[3].

Both relaxation and recombination losses reduce the values $P_{\max}^{\max} = I_{sc}V_{oc}$ and η_i proportionally. In work [11] by Shockley and Queisser it was shown that $\eta_i = (1 - \text{Loss}\,2)(1 - \text{Loss}\,3)$. In the absence of optical loss for a SC with the ideal fill factor, internal quantum efficiency of the SC is equal to $P_{\max}^{\max}/P_{\text{inc}}$. For advanced silicon SCs Loss 2= 0.33 and Loss 3 = 0.05, which gives $\eta_i \approx 0.63$. Since c-Si SCs became available in 1983, $\eta_i \approx 0.59$ [7], and in 36 years it was increased only slightly. We may conclude that the internal quantum efficiency value is, nowadays, close to its practically achievable limit.

Now, let us estimate the maximal achievable value of the *overall efficiency* of any SC based on a given PV material. In the literature, there are different definitions of this parameter. So-called *ultimate efficiency of a SC* introduced by Shockley and Queisser normalizes the electric power produced by the unit area of a SC not to the real power flux of the incident sunlight but to the *useful* (high-frequency) part of the solar power spectrum *absorbed in the PV layer*. In other words, the ultimate efficiency does not take into account Loss 1 and optical loss. Also, it does not take into account the Ohmic loss which arise in the contact areas, due to realistic impurities of materials and other imperfections of a real SC. For advanced silicon SCs having $FF_{\max} = 0.85$

---

[3]One often considers also the spectral internal quantum efficiency – that referred to the unit interval of wavelengths within the solar spectrum. This value is more dispersive than the spectral photoelectric response because the spectral density of Loss 2 and Loss 3 are both frequency-dependent.

we have $\eta_u = FF_{\max} \cdot \eta_i \approx 0.5$.

The ultimate efficiency is not a realistic target value for a designer of a SC based on a given PV material. *Maximal achievable efficiency of a SC* in its most actual definition takes into account all inevitable losses omitted in η_u. Among them, the optical loss is the main one. A solar panel even in a big power station called *solar power plant* cannot rotate after the Sun. Such rotation in the terrestrial conditions would take a too significant part of the output power. Therefore, the angle of sunlight incidence may vanish only on the midday and varies during the daytime up to the nearly grazing incidence. Optical efficiency OE is the mean value of the integral absorption coefficient of power in the PV layer. Mean value implies the averaging over the incidence angles during the daytime. Therefore, in the definition of the maximal achievable overall efficiency

$$\eta_{\max} = \eta_{sp} \cdot \eta_u \cdot VF \cdot CCF \cdot OE_{\max} \qquad (10.1)$$

$OE_{\max}$ is obviously smaller than unity. Also, in (10.1) VF called *voltage factor* and CCF called *current collection factor* are factors which take into account the aforementioned voltage and current losses, respectively. For most advanced SCs operating on standard terrestrial conditions OE is nowadays equal to 0.85 (see below). It is reasonable to assume that it can hardly be made higher than 0.90. For silicon SCs with the optimized geometries of the PV layer and electrodes VF and CCF can be as high as $VF \approx CCF \approx$ 0.95. Since for silicon SCs $\eta_{sp} = 0.81$ and $\eta_u = 0.5$, we obtain adopting $OE_{max} = 0.9$ and $VF = CCF = 0.95$ that the maximal achievable overall efficiency of silicon solar photovoltaics in civil terrestrial applications is equal to $\eta_{\max} = 0.3$ [12]. In the literature, this value is sometimes also called the Shockley-Queisser limit. Some authors, in order to stress that this value is different from the ultimate efficiency, originally calculated by Shockely and Queisser, call $\eta_{\max}$ *practical* Shockley-Queisser limit.

Practical limit efficiency $\eta_{\max} = 0.3$ is not the highest one determined for usable PV materials. For SCs based on purified germanium and for those based on so-called *metal-organic perovskites* the practical Shockley-Queisser limit was estimated as nearly equal to 40% [16–18]. For SCs based on amorphous semiconductors – the most popular PV material used in flexible thin-film SCs – this limit is estimated as $13 - 15\%$ [19, 20]. Below, we will explain why this low limit still keeps a good market perspective for amorphous PV materials.

An advanced silicon SC in 2009 manifested the record overall efficiency $\eta = 0.25$ [21]. However, this SC was fabricated in a laboratory. For the similar samples industrially adapted for mass production this record value could not be achieved. Moreover, this record efficiency was measured for the normal incidence of sunlight when A_{PV} was close to unity. The mean (daytime-averaged) optical efficiency OE of that SC was not published but should have been of the order of 0.8. Potential improvement of that SC has been mainly related to the possibility to further reduce the daytime-averaged optical loss. The other possibilities to enhance it without a drastic increase of the fabrication cost were exhausted [23]. This why since 2009 most efforts of researchers exploring this area have been invested namely into nanostructured ARCs decreasing the reflection loss of silicon SCs for the oblique incidence of sunlight. However, nanostructures decreasing the optical loss are topical not only for silicon solar photovoltaics. They are especially topical nowadays for *thin-film solar cells*. Below we will see why it is so.

10.2.5 On multijunction solar cells

As it was already mentioned, SCs with an effective split of the solar spectrum can beat the restriction of 30% minimum for Loss 2 and 19% minimum for Loss 1. Therefore, in this way one may overcome the Shockley-Queisser limit for silicon SCs. A multijunction (cascaded) SC represents an effective series connection of relatively narrow-band PV cells (called PV cascades), separated from one another by nanometer-thick layers of an insulator through which the photocurrent flows practically without losses due to the tunnel effect. Each partial cell of this monolithic structure absorbs a dedicated sub-band of the solar spectrum. In Fig. 10.6(a) we show an example of multijunction SCs reviewed in [20]. Physically, it comprises three PV diodes connected in series by *tunnel junctions*. The top SC converting the high-frequency part of the solar spectrum is based on InGaAs.

In Fig. 10.6(b) the solar spectrum is depicted as split into three parts corresponding to three cascades of the multijunction SC. The gray area corresponds to the solar spectrum marked as $AM1.5$ (this notation corresponds to a typical orbit of the Earth satellites). The part of the solar spectrum highlighted by blue is the part of the low-frequency power spectrum absorbed by the top cascade. GaAs beams are added here for a better Ohmic contact of the top cell with the metal microstrips. GaAs forms a good contact with both InGaP and metal (Al) preventing formation of parasitic Schottky diodes on

the interfaces Al/InGaP (that would reduce V_{oc} and increase surface recombination). So-called *window layer* and so-called BSF layer (*back-surface-field layer*) suppress surface recombination reducing Loss 3 to its minimal value about 5%. The second effective PV diode converting the middle part of the spectrum is based on InGaAs. The part of the spectrum absorbed by the middle cascade is highlighted by green. The third cascade converting the low-frequency part of the spectrum (the absorbed portion is highlighted by magenta) is a *heterojunction* PV diode based on three PV layers: InGaAs, InGaP, and Ge that form a unique *polycrystalline* structure. It is clear that the overall efficiency of this SC is mainly restricted by parasitic absorption of the sunlight in the non-dedicated cascades. The useful (PV) absorption is lowest in the bottom PV diode whose optical efficiency is close to 0.5 due to parasitic absorption of the red light in two PV cells located above.

In this SC Loss 2 reduces from 35-40% typical for a silicon SC to about 10%. Moreover, the consolidated operation band covers now the IR part of the solar spectrum, and Loss 1 is reduced so that the spectral efficiency exceeds 90%. The optical efficiency of this SC is close to 0.7 (due to high parasitic absorption in the cascades) and the overall efficiency is about 0.25 [20]. It was the record value for SCs in the 1970s.
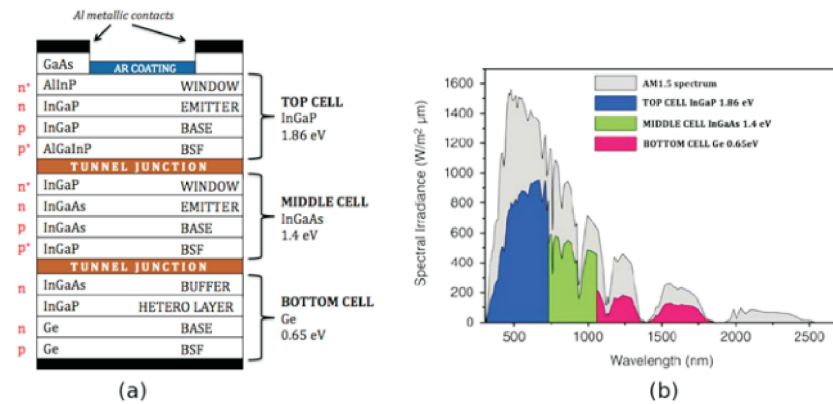
Figure 10.6: (a) Multijunction SC with a monolithic design and multilayer anti-reflective coating in between the microstrips forming the top contact. (b) Three bands of the solar spectrum (those centered at λ =520 nm, λ =770 nm and λ =1440 nm, respectively) are converted into electricity by three effective single-junction SCs entering the multijunction structure. Reprinted from [12] with permission of the editors.

Monolithic multijunction SCs are very expensive and, therefore, are not competitive as electricity sources for civil terrestrial applications even in huge solar power plants. However, in space (and military) applications the price of electricity is not the main issue. Therefore, the development of such SCs since 1970s has continued and resulted in 46% of their modern overall efficiency [24].

Notice that their optical efficiency, nowadays, exceeds 90% because the satellite SCs (arrayed in big panels) rotate so that to be orthogonal to the sunlight flux all the time when the satellite is illuminated (beyond the shadow of the Earth). This rotation offers low reflection losses but is specific for the space orbit where the rotation of a large mass does not consume an important part of the produced electric energy. The terrestrial SCs we consider below are stationary, as we have already discussed.

Here we finish the introductory section and in the next section we will mainly concentrate on the issue of reflection losses. This issue is either fully omitted or very weakly concerned in available books on SCs.

10.3   Optical efficiency of solar cells with an optically thick photovoltaic layer

If the PV layer is optically thick, meaning that it is thicker than the penetration depth of the sunlight, the light is absorbed before it reaches the bottom electrode. In this case, there are two components of the optical loss. One component is parasitic (non-PV) absorption in the heavily doped contact layers which is absent in interdigital-back-contact (IBC) SCs. The second (and main) loss component is the reflection or backscattering loss. Let us consider the problem of this loss revisiting Fig. 10.6(a) where an obsolete multijunction SC is depicted. First, we see that the top surface of this SC is not completely illuminated. A part of the surface is shadowed by the current-collecting electrode representing a mesh of metal microstrips. The minimal width of the microstrip is restricted by the mesh impedance, which should be enough low for effective carriage of current. This impedance growth for very tiny contacts [8], and, practically, the microstrips should have the width of the order of $w = 10\,\mu$m or more [7]. The mesh impedance depends also on the mesh period a. If this period is too large, the effective paths of the charges (the lines of the photocurrent bulk density) condensing around the

microstrips elongate too much and their lengths become large compared to the thickness of the PV layer. It results in growth of both bulk recombination and Ohmic losses in the SC.

Therefore, there is an optimal ratio w/a representing a compromise between the minimal optical and minimal bulk recombination and Ohmic losses. For example, when $a = 10w = 100\,\mu$m, CCE and VF are both close to 0.95 (high enough), whereas the bulk recombination and Ohmic losses in the SC are nearly the same as if the photocurrent lines were vertical. Therefore, a typical design of a SC with a front metal contact implies an array of parallel microstrips of the width $w = 10$ microns and the period about 0.1 mm. This design implies an irreducible component 10% of optical loss due to the shadow. Special solar concentrators were developed in 1960–1980s to focus the sunlight into the open areas between these microstrips [20]. However, the cost of these concentrators made the solar electric energy too expensive. Therefore, the term $w/a \approx 0.1$ practically inevitably enters the reflection loss of SCs with metal top electrode. For silicon SCs with a front contact mesh this irreducible loss is as high as 15% due to the parasitic absorption in the heavily n-doped silicon in the top part of the PV layer.

In modern silicon SCs there is no front mesh. In the case of the IBC design the optical loss related to parasitic absorption in heavily doped layers is negligible. The PV layer of a crystal-silicon SCs is optically thick and the sunlight is absorbed before it reaches the heavily doped nano-regions [22]. Since the factor w/a is removed from the optical loss of the SC with back contacts, only the reflection loss of the open surface remains.

As we have mentioned, this reflection loss factor grows versus the incidence angle θ. In the absence of an advanced antireflection structure it grows rapidly with θ when θ becomes large. However, before inspecting this angular dependence, we need to understand how the antireflection coating (ARC) operates for the normal incidence. Basically, the antireflection coating is a matching device, whose purpose is to ensure that the input impedance at the input surface is equal to the free-space impedance. As is well known, broadband matching can be realized with multi-layered stacks of low-loss dielectrics. However, we should take into account that multilayer ARCs of ten or more stacked nanolayers (used in satellite SCs because they should be ultra-broadband and very efficient) are never used in civil terrestrial applications. The first reason why multilayer ARCs are replaced in commercial SCs by single-layer antireflectors is simple: the high costs of multilayer ARCs. The second reason is not so simple. It is the presence of the so-called *front*

glass or another macroscopically thick laminate protecting the surface of the ARC from atmospheric abrasion. Below we will see how this factor erases the advantages of multilayer ARCs.

10.3.1 Single-layer antireflection coating and the impact of the front glass

In an obsolete silicon SC developed in work [25] the ARC was a 80 nm-thick layer of MgF (refractive index $n = 1.37$). If MgF is not covered by a front glass, the open area of this SC reflects only 8% of the normally incident sunlight power [25]. When this SC is covered by a front glass layer ($n_{rmglass} = 1.48$), this reflectance increases to 12%. Below we deduce both these values.

Let a layer (1) of thickness d_1 with refractive index $n_1 = \sqrt{\varepsilon_1}$ (here ε_1 is its relative permittivity in the optical range) be placed on a semi-infinite substrate (2) with refractive index $n_2 = \sqrt{\varepsilon_2}$. For a normally incident plane wave of frequency ω (the wave number in free space is $k_0 = \omega/c$) the surface impedance on top of this structure can be found from the transmission-line equation (e.g., [26]):

$$Z_s = Z_1 \frac{Z_2 + jZ_1 \tan \gamma_1 d_1}{Z_1 + jZ_2 \tan \gamma_1 d_1}, \qquad (10.2)$$

where γ_1 and $Z_{1,2}$ are the wave number in medium 1 and the wave impedances of media 1 and 2, respectively:

$$\gamma_1 = k_0 n_1, \quad Z_{1,2} = \sqrt{\frac{\mu_0}{\varepsilon_0 \varepsilon_{1,2}}} = \frac{Z_0}{n_{1,2}}. \qquad (10.3)$$

Here Z_s means the input impedance of a transmission line (whose role is played by the layer d_1) and Z_2 is the load impedance of this transmission line. In general, Z_2 is the surface impedance of the bottom interface, but the substrate is assumed to be semi-infinite and the surface impedance of a half-space for the normal incidence is equal to the wave impedance of the medium [26].

If the incidence is oblique ($\gamma_1 = k_0 \sqrt{\varepsilon_1 - \sin^2 \theta}$, where θ is the incidence angle), formula (10.2) is still applicable with replacements $Z_{1,2} \to Z_{1,2}^{TE,TM}$ for TE-polarized (or s-polarized) and TM-polarized (or p-polarized) incident waves, respectively. Here

$$Z_{1,2}^{TE} = Z_{1,2} \frac{n_{1,2}}{\gamma_{1,2}}, \quad Z_{1,2}^{TM} = Z_{1,2} \frac{\gamma_{1,2}}{n_{1,2}}, \qquad (10.4)$$

and, of course, $\gamma_2 = k_0\sqrt{\varepsilon_2 - \sin^2\theta}$ [26].

If medium 2 is a layer having a finite thickness d_2, formula (10.2) is generalized by replacement of the impedances $Z_2^{TE,TM}$ by the surface impedance of layer 2. The last impedance refers to the interface of media 1 and 2 and is calculated by the same transmission-line formula where the surface impedance of the substrate (layer 3) replaces that of layer 2. This approach allows us to deduce the surface impedance of an arbitrary number of stacked layers [26, 27].

For the normal incidence the amplitude reflection coefficient ρ and power reflectance R are easily found from the surface impedance:

$$\rho = \frac{Z_s - Z_0}{Z_s + Z_0}, \qquad R = |\rho|^2. \tag{10.5}$$

Formula (10.5) generalizes for the oblique incidence by substitutions $Z_0 \rightarrow Z_0^{TE,TM}$, where $Z_0^{TE} = Z_0/\gamma_0$, $Z_0^{TM} = Z_0\gamma_0$, and $\gamma_0 = k_0\sqrt{1 - \sin^2\theta} = k_0\cos\theta$ [26].

The normal-incidence reflectance in (10.5) vanishes under the matching condition $Z_s = Z_0$ that occurs in accordance to (10.2) when $n_1 = \sqrt{n_2}$ and $\gamma_1 d_1 = \pi/2$. The layer having such thickness and refractive index is called *quarter-wave plate* also called *simple antireflector*. For frequencies slightly lower than $\omega_0 = \pi c/2n_1 d_1$ the normal-incidence reflectance remains very small.

A simplified model of the silicon refractive index (adequate in the red and inter-band frequency ranges) neglects frequency dispersion of its refractive index, assuming that it equals $n_2 = 3.61$. For this medium the best simple antireflector is a quarter-wave plate of silicon nitride having $n_1 = 1.9$. In the red band R of the c-Si half-space covered with an antireflector of SiN is practically zero and R attains 0.1 only in the blue band of the solar spectrum. This property of an antireflector makes the operation of this simplest ARC quite broadband. In fact, it is really so in spite of the frequency dispersion of silicon (or any realistic PV material underlying the antireflector). Though this dispersion is detrimental for the antireflection operation of a quarter-wave plate (increases the mean value of R), small dielectric losses accompanying this dispersion are favorable for this operation [30]. In fact, only reasonably small losses with $Re(n_2) \gg Im(n_2)$ are favorable. Too high dielectric loss factor in the PV material increases reflectance [30]. Obviously, losses in the antireflection layer are always harmful for optical efficiency [29, 31].

Thus, for silicon $n_2 \approx 3.6 - j0.3$ without a front glass the practically optimal simple antireflector is a layer of silicon nitride of thickness $d_1 = \pi/2\gamma_1 = 76$ nm [29]. If we average R with the weight $S(\omega)$ over the whole operation band of the silicon SC $[\lambda_{\min}, \lambda_g]$, we obtain an even smaller value $R_{\text{int}} \approx 0.04$, i.e., the optical loss in the open area of the SC for the normal incidence is only 4%. Taking into account the shadow caused by the front contact mesh we obtain the optical loss factor for the normal incidence as $OL = 10\% + R = 14\%$. If the antireflector is performed of MgF as in [25], we obtain from (10.5) $R_{\text{int}} \approx 0.08$ because MgF has the refractive index $n = 1.37$ which is not optimal. Then for the normal incidence we have $OL = 18\%$.

Notice that the value $R_{\text{int}} \approx 0.04$ is achieved using an antireflector performed with nanometre precision. Making one layer with such precision is not very expensive for mass production. Costs drastically grow when the number of stacked nanolayers increase [23, 31, 32]. However, even for a single nanolayer it is impossible to maintain this precise thickness during many years of operation because the solar cell is under influence of such atmospheric factors as dust, rain, and even hail. Atmospheric abrasion decreases the thickness of the antireflector resulting in about 30% degradation of the SC overall efficiency per year [15]. That is why silicon SCs utilizing antireflectors are either encapsulated by a protecting laminate or covered by a macroscopically thick layer of glass. This protecting layer is prepared without micron or submicron precision, i.e., its thickness D has statistic deviations from the mean value which are larger than λ.

Let us elucidate the role of the front glass in the optical loss. First, let us see that the front glass reduces R even in the absence of an antireflector. Really, the normal reflectance of bare Si at $\lambda = 600$ nm in accordance to (10.5) is equal to

$$R_{Si} = |\rho_{Si}|^2 = \left| \frac{n_2(\lambda) - 1}{n_2(\lambda) + 1} \right|^2 = 0.33, \tag{10.6}$$

whereas the amplitude reflection coefficient of a bilayer formed by a glass layer of an arbitrary thickness D and typical refractive index $n_{\text{glass}} = 1.5$ on the Si half-space can be calculated as

$$\rho = \rho_{\text{glass}} + (1 - \rho_{\text{glass}}^2)\rho_{Si/\text{glass}} e^{-2j\gamma_{\text{glass}}D}. \tag{10.7}$$

Formula (10.7) is the so-called *two-ray approximation* [28]. The first term in (10.7) corresponds to the ray reflected from the protecting glass to free

space. The second term in (10.7) corresponds to the ray transmitting into glass with the amplitude transmission coefficient $1 + \rho_{\text{glass}}$, passing the optical path $\gamma_{\text{glass}}D$ towards the Si substrate, reflecting from Si with the reflection coefficient

$$\rho_{Si/\text{glass}} = \frac{n_{Si} - n_{\text{glass}}}{n_{Si} + n_{\text{glass}}}, \tag{10.8}$$

passing after this reflection the backward optical path $\gamma_{\text{glass}}D$ and, finally, transmitting to the air with the amplitude transmission coefficient $1 - \rho_{\text{glass}}$. Multiple internal reflections in the glass layer of thickness D can be neglected because the macroscopic layer cannot be perfectly flat – its interfaces are wavy [29]. Thus, formula (10.7) gives for the power reflectance $R = |\rho|^2$:

$$R = \rho_{\text{glass}}^2 + (1 - \rho_{\text{glass}}^2)^2 \rho_{Si/\text{glass}}^2 + 2\rho_{\text{glass}}^2(1 - \rho_{\text{glass}}^2)\cos(2\gamma_{\text{glass}}D). \tag{10.9}$$

Since the front glass is a macroscopic layer and its thickness randomly varies over the area, parameter D is stochastic. The statistically averaged value for R implies the averaging over possible values of D. Since the mean value of the cosine function is zero, the statistic averaging of (10.9) does not contain a term describing interference effects between rays 1 and 2. Omitting the last term in (10.9) and substituting $\rho_{\text{glass}} = (n_{\text{glass}} - 1)/(n_{\text{glass}} + 1)$ we deduce for the reflection loss:

$$R = \left(\frac{n_{\text{glass}} - 1}{n_{\text{glass}} + 1}\right)^2 + \left[\frac{2n_{\text{glass}}\rho_{Si/\text{glass}}}{(n_{\text{glass}} + 1)^2}\right]^2. \tag{10.10}$$

The substitution of (10.8) at $\lambda = 600$ nm into (10.10) gives $R \approx 0.21$ which is smaller than $R_{Si} = 0.33$. This improvement refers to all frequencies and it was confirmed by comparison with experiments in [29].

Introducing a nanolayer with the optimal refractive index $n = \sqrt{n_{\text{glass}}n_{Si}} = 2.3$ (e.g., zinc oxide) and the optimal thickness $d = 82$ nm (a quarter-wave plate at $\lambda = 600$ nm), sandwiched between silicon and glass media we nullify the second term in (10.10) at $\lambda = 600$ nm and make it rather small in the whole operation band. Really, in this case we should replace $\rho_{Si/\text{glass}}$ by the reflection coefficient of an antireflector (10.5), where Z_0 is replaced by $Z_{\text{glass}} = Z_0/n_{\text{glass}}$, and Z_s is given by (10.2) with substitutions $Z_1 = Z_{\text{ZnO}}$, $n_1 = n_{\text{ZnO}}$. ZnO layer of thickness $d = 82$ nm grants us $R_{\text{int}} \approx R_{\text{glass}} \approx 0.05$, i.e., almost the same value of the open-area reflection loss as that obtained for a silicon nitride antireflector without glass. For an antireflector of MgF utilized in [25] the second term in (10.10) does not vanish at any λ. In this

case, after averaging of R over the solar spectrum we obtain $R \approx 0.12$, i.e., an antireflector of MgF is not recommended also in the presence of front glass.

The reflectance of the front glass, given by the first term in (10.10), definitely suffers from the atmospheric dust and other factors. From another point, this reflectance can be further decreased if we make the refractive index of the front glass nonuniform in the vertical direction. A slab of porous glass whose porosity varies with the depth can be modelled as a composite slab whose reflective index varies across the slab. Practically, one can achieve $n_{\text{bot.}} = 1.5$ near the bottom interface and $n_{\text{top}} = 1.4$ near the top interface [28, 29]. In this case, the front glass reflectance reduces from 0.04 to 0.028 and the antireflector remains the same because $n_{\text{bot.}}$ does not change. In this case the integral normal reflectance of the whole SC is nearly 0.03 – almost equal to that of the front glass. Self-cleaning functionality engineered for such porous glasses is described in [33].

In 1973 an ARC called the *moth-eye texture* was suggested in work [34] for better suppression of reflection from optical glasses. Instead of a porous glass plate one can use a specially prepared composite layer whose effective refractive index changes smoothly versus the vertical coordinate. On the top surface it is equal to $n = 1$, i.e., the front reflection is presumably eliminated. Below we will inspect this issue in more detail studying the *moth-eye ARCs*.

10.3.2   Oblique incidence and daytime-averaged optical loss

In the case of the incidence under an angle θ, the reflectance of an air-glass interface can be found as

$$\rho_{\text{glass}}^{TE} = \frac{\cos\theta - \sqrt{n_{\text{glass}}^2 - \sin^2\theta}}{\cos\theta + \sqrt{n_{\text{glass}}^2 - \sin^2\theta}}, \tag{10.11}$$

which gives $(\rho_{\text{glass}}^{TE})^2 \approx 0.17$ for $\theta = 60°$ and $(\rho_{\text{glass}}^{TE})^2 \approx 0.32$ for $\theta = 70°$. For the TM-polarization the reflection coefficient is not monotonous versus θ due to the Brewster effect:

$$\rho_{\text{glass}}^{TM} = \frac{n_{\text{glass}}^2 \cos\theta - \sqrt{n_{\text{glass}}^2 - \sin^2\theta}}{n_{\text{glass}}^2 \cos\theta + \sqrt{n_{\text{glass}}^2 - \sin^2\theta}}. \tag{10.12}$$
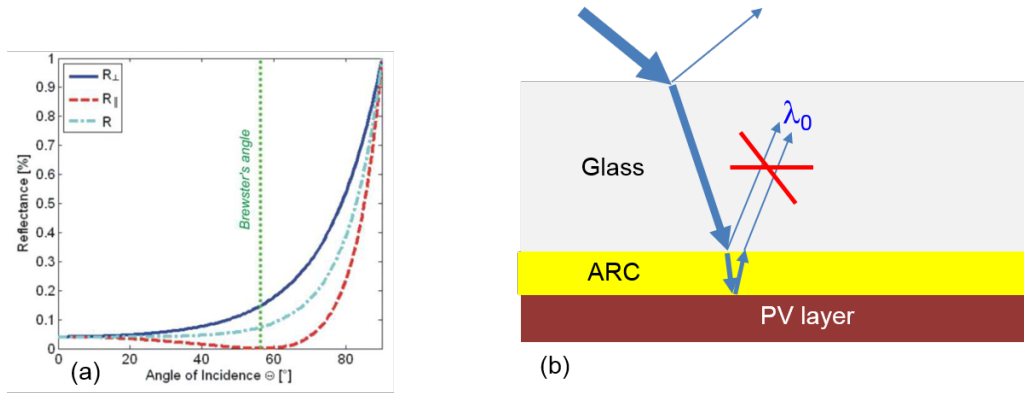
Figure 10.7: (a) Integral reflectance of sunlight from a usual glass layer: TE-polarization (solid curve), TM-polarization (dashed curve) and unpolarized light (dash-dotted curve). Reprinted from [35]. Unrestricted use of this open-access article is permitted. (b) The physics of antireflection is based on the mutual cancellation of partial reflections from the top and bottom interfaces of the ARC layer.

From these formulas (applicable at any optical frequency) we find the averaged power reflectance $R_{\mathrm{glass}} = \left(|\rho_{\mathrm{glass}}^{TE}|^2 + |\rho_{\mathrm{glass}}^{TM}|^2 \right)/2$ corresponding to the non-polarized light. R_{glass} as well as the polarized reflectances $[\rho_{\mathrm{glass}}^{TE}]^2$ and $[\rho_{\mathrm{glass}}^{TM}]^2$ are shown in Fig. 10.7(a). The curves corresponding to the case when R_{glass} is replaced by the integral (over the solar spectrum) reflectance R_{int} of the front glass with an ARC inserted between the front glass and the PV layer do not visually differ from the curves obtained for a semi-infinite glass at any λ [36]. The physics of antireflection is based on the mutual cancellation of partial reflections from the top and bottom interfaces of the ARC layer, as shown in Fig. 10.7(b). Realization of the effect of destructive interference demands the equivalence of the magnitudes of the two reflected waves and their opposite phases. Their exact cancellation is possible only at one wavelength λ_0 where the reflectance of the whole structure equals to that of the front glass. However, for the normal incidence, the reflectance turns out to be close to that of the front glass in a rather broad band of wavelengths. For the oblique incidence the performance of this simple ARC is not so broadband.

To perform the averaging over the incidence angle θ which varies during the daytime we should specify the maximal incidence angle θ_{max} correspond-

ing to the daytime edges. There is no agreement in the solar photovoltaic community which value of θ_{max} should be adopted. Below we assume that $\theta_{max} = 80°$ – in this case our calculations better fit the literature data than in the case if the choose $\theta_{max} = 90°$. With our choice of θ_{max}, the daytime-averaged reflectance of the front glass turns out to be equal 0.095. This value describes the effective averaged reflectance of the open area of a SC. Also, in the daytime-averaged optical loss factor the shadow term w/a must be present which does not depend on θ. Thus, the expression for the mean (or effective) optical loss factor is as follows:

$$OL = \frac{1}{\theta_{max}} \int\limits_{0}^{\theta_{max}} R(\theta) \, d\theta + \frac{w}{a}. \tag{10.13}$$

For a c-Si SC with a front contact mesh $w/a = 0.1$ formula (10.13) gives $OL \approx 0.2$, i.e., the optical efficiency of a silicon SC with a front glass and a contact mesh equals to 80% in spite of the presence of an ARC. The use of a bilayer and even a multilayer ARC instead of a simple antireflector cannot give a real improvement because the presence of the front glass erases the advantages of a multilayer ARC. For SCs with interdigital back contacts the shadow factor w/a disappears. Then the mean optical loss reduces nearly twice, and we have $OL \approx 0.1$ [29, 36] (also the recombination loss decreases, though the Ohmic loss increases and current collection efficiency decreases, as we discussed above).

To further reduce the optical loss, researchers continue developments of transparent composite glasses (see e.g. in [44]). However, the progress in this field is modest and other technical solutions implying absence of the front glass have been found.

10.3.3 Moth-eye antireflectors

If we remove the front glass from the top of a solar panel, the lifetime of the latter reduces due to atmospheric abrasion. Meanwhile, the optical loss also reduces because the first term in (10.13) is removed. Nowadays, the companies working in solar photovoltaics, where the competition is very strong, struggle for every decimal part of a percent of the overall efficiency [18,23,24]. Therefore, a possibility to get rid of extra ten percents weights more than the theoretical decrease of the solar panel lifetime which will occur in the

future. This practical need stimulated studies of moth-eye ARCs replacing the glass cover on top of a SC.

This dielectric texture is quite similar to the moth-eye photonic crystal of cylindrical protrusions (see in Chapter 5). However, in contrast to the natural and photonic-crystal moth eyes having the periods of the texture within the interval $250 - 300$ nm, the period b of the moth-eye ARCs cannot exceed $150 - 200$ nm because the key prerequisite of homogenization of any composite structure is smallness of its constituents compared to the wavelength. Practically, the period of protrusions is equal to $80 - 100$ nm, whereas their height is $200 - 500$ nm. Next, the protrusions are not simple nanorods but have the shape of cones with smoothed tops [37–42].

In 1973, when the first moth-eye ARC was suggested in [34] as an ARC for optical glasses, the target was to achieve a vertical gradient of the effective refractive index from 1.5 to unity. However, needed manufacturing technology did not exist. Therefore, only a microwave model experiment confirming the governing idea was performed. Another implementation of this idea was suggested in work [43] and it was also realized at millimeter waves, at frequencies much lower than those of sunlight.

Nowadays, a moth-eye ARC can be fabricated, for example, using the so-called *nanoimprint lithography*. This method is based on the use of a once fabricated hard stamp of quartz. This stamp before losing the required quality can replicate many times, molding a lot of much softer surfaces than that of quartz, producing needed textures. This technology is affordable for the solar PV industry on condition of mass production. It allowed one to drop the idea of challenging optical composites suggested in [34] in favor of simple arrays of dielectric protrusions obtained by this lithography technique [38, 40, 41].

The operation of this array is qualitatively illustrated by Fig. 10.8. In the absence of front glass, it is reasonable to return to the consideration of a multilayer ARC, illustrated by Fig. 10.8(a). Its refractive index is stepwise along the vertical coordinate, as depicted in Fig. 10.8(b). The large number of layers gives a set of frequencies and angles for which the partial waves reflected from all the interfaces interfere destructively. The thinner are these layers and the larger is their number, the more broadband and more angularly stable is the antireflective operation. However, this way implies also an increase of fabrication costs: the thinner is a nanolayer the more fine precision is required, the larger is the number of layers, the more efforts are needed to ensure their flatness. This is the reason why the moth-eye geome-
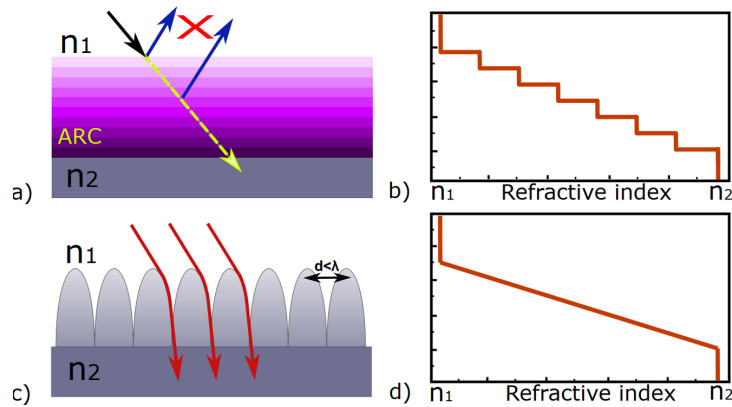
Figure 10.8: (a) A multilayer ARC grants several wavelengths at which the wave reflected by the top interface cancels out with that reflected by one of intermediate interfaces. Similarly, for several incidence angles the reflection can be suppressed. (b) The refractive index profile of the multilayer ARC is stepwise. (c) Moth-eye ARC performed as an optically dense array of properly profiled protrusions suppresses the reflection better than the multilayer ARC. (d) The effective refractive index of the moth-eye ARC smoothly varies in the vertical direction from n_1 to n_2. These four figures are drawn by the author after [42].

try shown in Fig. 10.8(c) was chosen for open-air ARCs. Roughly speaking, a moth-eye ARC behaves as a layer of an effective medium whose refractive index at a given horizontal plane is determined by the cross-section area occupied by the medium having the refractive index n_2. In the bottom part of the ARC it occupies the whole area, and the effective refractive index is equal to n_2. In the top part of the structure it occupies a small area and the effective refractive index approaches n_1. Thus, the effective refractive index of the moth-eye ARC can be thought to be the limit case of a multialyer ARC. The moth-eye ARC has no optical contrast at the effective top and bottom interfaces. If the situation illustrated by Fig. 10.8(d) were applicable to all frequencies and all incidence angles, this structure would be perfectly matched with free space, i.e., be reflection-free for all frequencies and incidence angles. Of course, this plot is an idealization – a moth-eye ARC is not an all-frequency and all-angle device, though it is much better than a simple antireflector.

In principle, a moth-eye ARC can be performed as a flexible nanotexture

of a transparent resin attached to the transparent top electrode of the SC by a submicron layer of a polymer glue having nearly the same refractive index n_2 as that of the electrode. However, this nanotexture is very vulnerable and needs to be covered by a macroscopically thick polymer laminate in order to operate in the open air. Such laminates, nowadays, have the refractive index $n = 1.34$ and grant the lifetime of a solar panel up to $1 - 3$ years [45]. For a moth-eye ARC of acrylate resin located on a silicon SC and protected in this way one obtained in [38] the mean reflectance nearly equal to 7%. Together with the shadow factor $w/a = 10\%$ we obtain $OL = 17\%$ for the optical loss in the sandwiched geometry of the SC. However, the improvement of the optical efficiency from 80% to 83% is not sufficient in view of the reduced lifetime.

If we want to either reduce the reflection loss or extend the life of a solar panel to $5 - 10$ years we should get rid of the laminate and perform the ARC from a hard material. For silicon SCs a month-eye ARC can be fabricated of silicon nitride [29, 37] or performed as modified surface of c-Si itself [39]. The moth-eye ARC of silicon nanocones exhibits a very low reflectance for the normal incidence and small incidence angles (less than 2% in accordance to [39]). However, for large angles θ the reflectance increases, and the mean value of the reflection loss is close to 10% (i.e., $OL \approx 20\%$ and there is no improvement compared to the simple ARC). Why it is so?

Unfortunately, the explanation of the operation of a moth-eye ARC in terms of a smoothly varying refractive index is simplistic and ignores the spatial dispersion effects. The spatial dispersion – dependence of the effective material parameters on the wave vector – may arise in regular arrays if the period is of the order of $\lambda/4$ or larger. This is the case of practically achievable moth-eye ARCs. Due to spatial dispersion the effective refractive index of a moth-eye ARC calculated for the normal incidence differs from that calculated for the oblique incidence. For small incidence angles θ this difference is minor. If the phase shift between two adjacent protrusions $k_0 b \sin \theta$ is smaller than unity (here $k_0 = 2\pi/\lambda$ is the free-space wave number), the interference of electromagnetic waves scattered by two adjacent protrusions is still negligible. In this case the array can be homogenized the same way as in the case of normal incidence. However, for large incidence angles when $k_0 b \sin \theta > 1$ the electromagnetic interference of the waves scattered by any two adjacent protrusions arises. This interference is not as strong as that resulting in the Fraunhofer diffraction maxima for the scattered field because $b < \lambda/2$. However, it is not negligible and disables the simplistic model of

the gradient refractive index. Practically, the concept of a smooth transition from n_1 to n_2 becomes meaningless for $\theta > \pi/4$.

The analysis of the spatial dispersion in moth-eye ARCs shows that the reflectance of the non-polarized light for typical periods $b = 80-150$ nm grows versus θ in the same way as for a flat interface [38]. The only difference is the lower value of this reflectance compared to the flat surface. If the material of the ARC has a low refractive index, the mean reflectance is low. This is the reason why for the ARC based on the acrylate resin having the refractive index 1.4 the mean reflectance equals to 0.07 and is mainly determined by the laminate. Silicon has the refractive index varying in the solar spectral range from 3.5 to 5 ($n_{Si} \approx 4.5-5$ in the blue and UV parts of the solar spectrum). Therefore, a silicon SC with a moth-eye ARCs is not more efficient during the daytime than a silicon SC with a simple antireflector and a front glass (which is more robust to the atmospheric factors).

However, not all wafer-type SCs are based on silicon. Epitaxial multicomponent semiconductors, such as GaInP, AlGaP, and GaAs are PV materials with similarly high photoelectric spectral response and lower refractive index, than that of c-Si. For these PV materials the use of hard laminate-free moth-eye ARCs turns out to be justified [40, 41]. Optimal moth-eye ARCs for such SCs require materials with the refractive index 1.7.

SCs based on epitaxial multicomponent semiconductors and gallium arsenide have a drastic difference in their optimal design as compared to silicon SCs. These semiconductors form a good Ohmic contact with transparent conductive oxides (TCOs). The conductivity of TCOs such as aluminum-doped zinc oxide (AZO), fluoride-doped tin oxide (FTO) and indium-doped tin oxide (ITO) is sufficiently high so that a nanolayer of thickness $\Delta = 80-100$ nm performed of such TCOs can collect the photocurrent flowing from the PV layer and redirect this current to the contact wires with the same current collection efficiency as a wire mesh having $w/a \approx 0.1$. The contact wires are located on the perimeter of the SC and create no shadow for the PV layer. In design, the optical loss OL does not contain the term w/a which was one of two main arguments against the sandwiched geometry of a silicon SC.

Unfortunately, TCOs are not ideally transparent within the solar spectrum, and a multiplicative factor describing the parasitic power absorption in a TCO layer replaces in (10.13) the term w/a. This factor for a given frequency $\omega \equiv k_0 c$ is equal to $\exp(-2\alpha\Delta)$, where $\alpha = k_0 \text{Im}\sqrt{\varepsilon_{TCO}}$) is the amplitude wave attenuation in a material with complex permittivity ε_{TCO} in the optical range and Δ is its thickness. The thickness value is chosen as

a compromise between the Ohmic loss due to a finite DC conductivity of a TCO and the aforementioned parasitic power absorption averaged over the solar spectrum. For optimal Δ the impact of the Ohmic loss in the TCO is negligible, whereas the parasitic optical absorption adds extra $5 - 6\%$ to the mean reflection loss (usually close to 10%).

As to SCs based on GaAs, they can be implemented with two technical solutions: with back contacts (like in modern silicon SCs) and with a top electrode. Both variants have nearly the same cost and efficiency. In the second variant, GaAs is covered by a nanolayer of transparent material serving for its chemical passivation (the window layer) and a front mesh of metal microstrips. Unlike chemical passivators used in silicon solar photovoltaics, this material of the window layer is electrically conducting. Materials of the window layer can be aluminium indium phosphate or gallium indium phosphate. They do not form surface states on the interface with GaAs because their crystal lattices allow a robust electric contact with GaAs. The optimal conductance of the window layer is achieved by its doping. Electric conductivity of the window layer is rather low in order to avoid high parasitic absorption of sunlight. Therefore, on top of it there is a contact wire mesh. However, the period a of this mesh is much larger than that of a similar silicon SC, and the shadow factor w/a is much lower. In the optimal design, the parasitic absorption and the contact mesh shadow result together in the same optical efficiency as that for multicomponent SCs with a moth-eye ARC [40, 41].

Thus, the mean optical loss of practical SCs utilizing moth-eye ARCs is nearly 15% where nearly 10% refer to the mean reflection loss and 5% refer to the parasitic absorption (or to the parasitic absorption and shadow). Though the improvement of the optical efficiency is modest (from 80% to 85%), it is easy to visually distinguish a SC covered with a laminate (e.g., front glass) from a SC with a moth-eye ARC on top. In the first case, the surface is bleaching and looks blue for large observation angles. In the second case, the solar panel is not bleaching and looks dark for any observation angle.

10.3.4 Black silicon

We have already mentioned that for silicon SCs a moth-eye ARC is not as efficient as for some other practical SCs because for large incidence angles θ regular silicon protrusions are not efficient. However, the governing idea of the effective refractive index varying in the vertical direction does not obviously requires a regular array of protrusions. An alternative – random –

implementation of this idea for Si-based SCs is called *black silicon.*
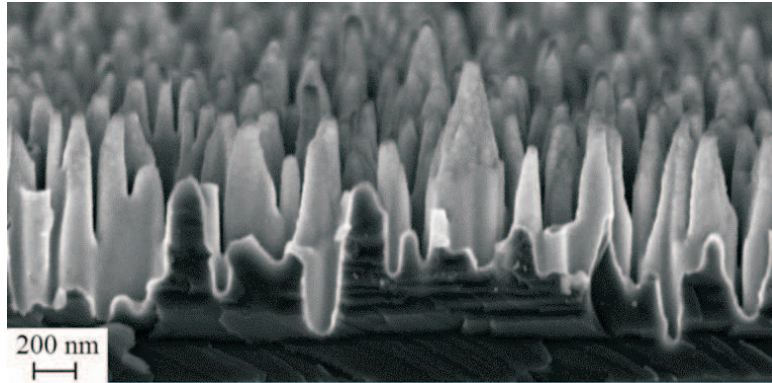
Figure 10.9: SEM micrograph of a black silicon surface developed in Aalto University. Reprinted from [47] with permission of the IEEE.

In [46] the authors suggested to use electrochemical etching or metal-assisted chemical etching that results in a stochastic roughening of the surface. In Chapter 9 we mention a similar technique for metal substrates, when it usually results in nearly hemispherical protrusions. Properly chosen technological parameters of electrochemical etching result for a semiconductor surface in a random but optically dense array of nearly conical protrusions. The mean values of the height and width of the cones can be $0.5 - 1$ μm and $100 - 200$ nm, respectively. Typical SEM pictures of such random arrays are presented in Figs. 10.9 and 10.10. The effective layer formed by such protrusions on top of a layer of c-Si can be described as an effectively continuous medium whose refractive index decreases from the bottom to the top due to the conical shape of the protrusions. When this structure is illuminated by obliquely incident light, spatial dispersion effects, very strong for periodical arrays, are negligible because in sub-wavelength random arrays there are neither constructive nor destructive interference effects.

A structure shown in Fig. 10.9 is a cheaper and more efficient ARC than the moth-eye arrays studied in papers [37, 39]. A demonstrator SC with this surface was fabricated in 2011 in Aalto University (the group of prof. H. Savin). Here, the surface of c-Si including all nanocorrugations was passivated by a $2 - 3$ nm thick layer of Al_2O_3 using atomic layer deposition. The material (corundum) resulting from this deposition does not contain even sub-nanometer pores, and a 2 nm-thick layer ensures high-quality passiva-

tion. Therefore, a drastic increase of the surface area is not accompanied by an increase of surface recombination. The daytime-averaged reflectance of this black Si does not strongly differ from the normal reflectance and is nearly equal to 4% [47]. In 2014 this achievement resulted in a record for the daytime-averaged efficiency of silicon solar cells $\eta = 22.1\%$ [48]. The record for the mean reflectance stood until 2017 [49]. However, the technical solution of [49] demands more expensive technologies.
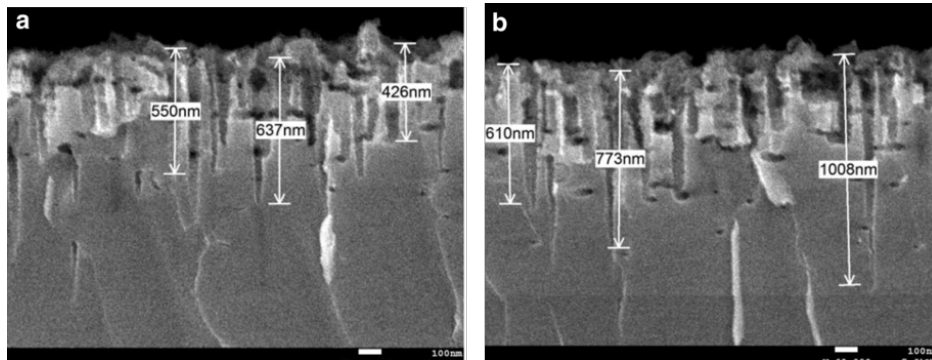
Figure 10.10: TEM micrographs of two samples (a and b) of black silicon obtained in Chengdu University using the metal-assisted chemical wet etching. Reprinted from [52] with permission of Springer Nature.

Sometimes, very elaborated patterns of black Si surfaces can be obtained using affordable nanochemistry methods, complementing nanophysical techniques. Combining nanophysics and nanochemistry, the authors of [50] obtained a 2D photonic crystal of free-standing 200 nm-thick Si nanorods of micron height prepared with the period $b = 500$ nm on top of a c-Si SC. This array was optimized via numerical simulations so that to minimize the reflectance at all angles from 0 to $\theta_{\max}$ corresponding to the daytime edge. It turned out to be feasible in the range $\lambda = 400 - 700$ nm. Later, the angular stability of the reflection loss factor for this regular type of black silicon was later confirmed experimentally [51]. However, the antireflective operation of this regular black silicon as well as the moth-eye silicon SC is not sufficiently broadband. The reflectance is high in the inter-band range, above 700 nm where c-Si is still an efficient PV medium and the solar spectrum is significant until $\lambda = 1050$ nm. An experiment has shown that this arrayed ARC does not reduce but increases reflection at $\lambda > 700$ nm compared to the bare flat interface of c-Si [51].

Black silicon ARC performed as random nanostructures are cheaper and very broadband. Profiles of two samples of black-silicon SC with self-cleaning property developed in [52] are presented in Fig. 10.10. The mean reflectance for one sample is nearly 10% and for the other one it is about 7%. However, it is just a plate of silicon with antireflective properties, and it is unclear which overall efficiency a corresponding SC could have.

Judging from media news, the record of the daytime-averaged conversion efficiency in the industrially adapted silicon-based photovoltaics in 2018 was $\eta_{PV} =$ 22.8%. It belonged to the Russian company *Hevel* [53]. This result was previously claimed for an experimental demonstrator tested in a laboratory [54]. However, it was achieved not with a conventional black-silicon SC but with a heterojunction SC based on different forms of silicon – polycrystalline (epitaxial) Si sandwiched between thin layers of c-Si (bottom) and amorphous silicon (top). In accordance to [54] this technology turned out to be affordable for commercialization. However, details of the fabrication process have not been published and therefore cannot be discussed here.

In these works, the antireflective properties are granted by a nanostructure similar to black Si. This random nanotexture is located on top of this SC and represents an array of ZnO protrusions. The textured layer of zinc oxide has two functionalities – that of the current collection and the antireflective one [55]. The trade-off between parasitic absorption in the top electrode and its Ohmic losses is resolved using an additional 70 nm layer of ITO, i.e., the photocurrent is collected by a bilayer electrode. The last one is backed by a nanolayer (thickness 20 nm) of a-Si, which has no PV functionality. Its purpose is to reduce surface recombination and to ensure the Ohmic contact of ITO and epitaxial silicon. The PV layer consists of epitaxial silicon and crystalline silicon sublayers, whose total thickness is sufficient for complete absorption of transmitted sunlight in one passage. For the normal incidence OL of this SC is close to 10% [55], where 6% refers to the parasitic absorption in the ITO layer and 4% corresponds to the contact wires $w/a = 0.04$ performed of silver. This sparse wire mesh is designed to decrease the Ohmic surface resistance like it was done in gallium arsenide SCs discussed above. For oblique incidence OL grows only slightly, and the mean optical efficiency of the SC nearly equals to 85% [54] (5% improvement compared to the conventional design).

Designers of this SC refer their heterojunction SCs covered by a roughened ZnO layer to the class of black-silicon SCs (see in [56]). Really, there are following common points: 1) the PV layer is made of solid silicon, 2) there

is no laminate or a front glass, 3) the surface is randomly nanotextured with a subwavelength period and is not bleaching for all angles, 4) the nanostructured surface of ZnO is similarly hard and robust to the atmospheric factors, promising several years of operation without noticeable degradation.

Notice, however, that the exploitation of such solar panels is not very cheap due to the necessity of daily water cleaning. It is especially important in polluted air where the dust contains so-called *particular matter* (particles whose size makes dozens of μm or even less) which attach to the zinc oxide and result in its abrasion [57]. As to black silicon structures with *self-cleaning functionality* suggested in [52], these SCs suffer of high surface recombination. For such black-silicon SCs Loss 3 exceeds 15% which does not allow them even to approach to the record mean efficiency 22%. Review papers [51,58] discuss a trade-off between the surface recombination level and the self-cleaning effect for black silicon. The dilemma was resolved only using expensive nanotechnologies [58]. Therefore, it appears that self-cleaning black-silicon SCs are hardly promising for commercialization [51].

At the time of writing, information on solar power plants built by Hevel Solar in different countries is available only from mass media (see e.g. in [59]) and confirms the daytime-averaged overall efficiency of 22% on sunny days. The same mean efficiency was achieved earlier (in 2016) by the American company *Silevo*[4]. This company used SCs based on so-called *oxide tunneling junctions* (see e.g. in [61–63]). Here we do not discuss the physics of these pioneering SCs which would deserve a separate monograph. It is enough to mention that these SCs utilize composite PV layers and do not refer to the class of black-silicon SCs though also comprise nanostructures.

Finally, note that in the scattered sunlight (cloudy weather) the electric output of black-silicon SCs drops by an order of magnitude. This refers to all SCs (see e.g. in [60]). The benefits of black-silicon solar photovoltaics and of that based on oxide tunneling junctions will be clear when the lifetime of solar panels in recently lounged solar power plants will be known and corresponding exploitation costs will be counted.

---

[4]Nowadays, it is a part of *Tesla*.

10.4   Antireflecting coatings formed by arrays of small spheres

An interesting affordable technique for manufacturing nanostructured ARC is presented in paper [64]. A densely packed array (monolayer) of micron or submicron sized spheres of silica (or another transparent dielectric) can be easily prepared on a flat dielectric or semiconductor surface because spheres better attach to the surface than to one another and may even self-assemble on the surface submerged in a colloidal suspension of such spheres (such colloids are inexpensive and available on the market with a great variety of particle diameters – from 100 nm to 10 microns). In order to prevent an occasional formation of multilayers of spheres one often uses the spin-coating technique. Then a monolayer structure results from the centripetal force which overcomes the mutual attachment of the spheres to one another.

After the monolayer has been obtained and water has been dried out, the whole surface can be encapsulated by a submicron film of a glue. In work [64] this glue was the spin-on glass, however, it can be also a polymer. This technique enables cheap fabrication of large-area ARCs with a regular nanostructure.

However, in what concerns reflection losses, these structures did not stand comparison with black silicon. Being placed on the surface of c-Si, these spheres are inefficient due to a high optical contrast between silica and silicon: the effective refraction index of the monolayer of silica spheres is nearly 1.4 whereas the refractive index of c-Si in the green range of the solar spectrum is about 4.0. We will discuss the applications of these ARC in the next section which is dedicated to *thin-film solar cells* (TFSCs).

10.5   Thin-film solar cells

In the previous section we saw that modern practical silicon SCs have a high fill factor that achieves $FF = 0.8 - 0.85$, the daytime-averaged optical efficiency achieves $A = 0.85 - 0.9$, and the mean overall efficiency is as high as $\eta_{PV} = 22\%$. We also saw that the current research in this field is not fundamental, but applied, and this applied research is a competition of numerous scientific groups for every decimal fraction of a percent. This struggle is mediated by the obvious condition of keeping low fabrication costs, safety of fabrication and absence of toxic waste.

However, there is an alternative branch of solar photovoltaics – that based on flexible sheets of PV materials. In this alternative area the potential for further improvement is huge, since in this technique SCs have an optically thin PV layer, insufficient to absorb the sunlight in one passage and even two passages. Techniques which prevent passage of the incident light across the PV layer before it has been absorbed, are called *light trapping*. Also, the high potential of improvement stems from the fact that basic PV materials of these SCs are either very inefficient (such as amorphous silicon) or not sufficiently stable in time (as synthetic perovskites).

10.5.1 Drawbacks, advantages and practical perspective of thin-film solar photovoltaics

Let us understand why TFSCs are practically interesting. Though advanced silicon SCs, such as produced by Silevo and Hevel, justify their cost in one year (whereas their lifetime is longer), they are not very attractive for domestic use. They are heavy and hard, requiring mechanically robust supports. Moreover, they are quite fragile and can be occasionally (or intentionally) broken. Meanwhile, TFSCs can be fabricated as light-weight flexible films. Flexibility makes them compatible with the so-called *roll-to-roll fabrication technique*, that minimizes fabrication costs along with the growing market. Additionally, this technique allows one to fabricate variable-area solar panels [19]. Finally, a flexible film is conformable to curved surfaces and does not spoil the appearance of a tile roof.

A very important type of TFSCs commercialized in 1970s (as a charging source for pocket calculators) were SCs based on amorphous silicon [19]. The Shockley-Queisser overall efficiency and the ultimate efficiency of a-Si TFSCs (13% and 42%, respectively, in accordance to [65]) are noticeably worse than those of its crystalline counterpart (30% and 50%, respectively). This is so due to high intrinsic losses (especially Loss 1) and low open-circuit voltage.

Loss 1 is high because the bandgap wavelength of a-Si is almost twice shorter than that of c-Si: it lies within the interval $\lambda_g = 600 - 700$ nm depending on the explicit design (λ_g depends on the static electric field in the depletion region). If $\lambda_g = 650$ nm, as it occurs in the most part of a-Si SCs, about one half of the incident solar power is lost, and the spectral efficiency is only $\eta_{sp} = 50\%$. Next, the mobility of the minor charge carriers in a-Si is much lower than their mobility in the usual (crystalline) silicon.

This drawback implies low drift velocity and small diffusion length of the carriers. Recall, that the time in which most of minor carriers pass through the doped bulk part to the corresponding electrode must be shorter than their lifetime. Otherwise, most part of the photocurrent carriers will recombine that will result in huge values of Loss 3. Therefore, low drift velocity of the carriers requires a smaller thickness of the PV layer. Usually, the thickness for the PV layer of a-Si is no more than 400 nm, and the PV diode cannot be a p-n one. First, in the doped a-Si layer minor charges are very slow and high recombination restricts the total thickness of these layers by maximum 100 nm. Second, in the p-n junction of a-Si the harmful Franz-Keldysh effect (see above) is too strong. Therefore, instead of a p-n junction one fabricates p-i-n diodes, where the typical thickness of the doped parts is as small as $30 - 60$ nm, and the intrinsic layer at the center has the thickness $200 - 350$ nm. The total thickness of the PV layer $300 - 400$ nm is not sufficient for absorption of solar light before it reaches the bottom electrode. Therefore, in the past, one fabricated an intrinsic a-Si layer with the thickness of the order of 1 μm (see e.g. in [67]). In these SCs Loss 3 exceeded 60% and the overall efficiency was about 2.5%.

If the thicknesses of all three sublayers are chosen to maximally reduce Losses 2 and 3 (and the doping level in the p- and n-sublayers is also optimal, namely, the minor carriers concentration is equal to $(2 - 3) \cdot 10^{18}\, cm^{-3}$ in these sublayers), Loss 2 and Loss 3 are reduced so that their sum does not exceed 30% [19]. However, the fill factor of a-Si in these best SCs attains 0.52 that restricts the ultimate efficiency and the practical Shockley-Queisser limit calculated using formula (10.1) by the values $\eta_u = 0.42$ and $\eta = 0.21$, respectively [66]. At a first glance, these numbers are promising. However, in these calculations, the optical efficiency is assumed to be equal 100%. Moreover, even neglecting the optical loss this estimate was too optimistic because Ohmic losses which are especially high in the contact area can hardly be negligible. Unlike its crystalline counterpart, a-Si does not form a good electric contact even with polished metal. Notice, that the polished metal cannot be flexible and is prohibited if flexibility is required. For flexible TFSCs, the back electrode is performed of a flexible metal foil electrically connected to a-Si by an intermediate contact material, such as *conductive paste* – carbon or graphite paste with copper inclusions. Alternatively, it can be a layer of a semitransparent conductive metal oxide such as doped ZnO. These materials possess noticeable optical losses. The thickness of the contact material is chosen as a compromise between parasitic absorption of

sunlight in the back electrode and its Ohmic resistance. Therefore, the overall efficiency suffers of both Ohmic loss and optical loss in the area of the back electrode.

As to the top electrode in TFSCs, it is usually performed of a TCO (AZO or ITO, in perovskite SCs – from FTO). If it is too thick, parasitic absorption makes the optical efficiency of the SC very low. If it is too thin, the Ohmic resistance of this electrode (recall that the current flows in it horizontally) strongly exceeds the internal resistance of the PV layer and too much of the generated electric power is dissipated. The optimized TCO layer for a TFSC has the thickness $70 - 80$ nm and the parasitic absorption in it subtracts $6 - 8\%$ from the optical efficiency. The Ohmic resistance of such optimized electrode is comparable with the internal resistance of the PV layer. It both bottom and top electrodes with the optimized parameters $30 - 35\%$ of the output power is lost.

Therefore, the maximally achievable overall efficiency reduces practically from 0.21 to nearly $0.134 - 0.139$. If we further take into account that the maximally achievable optical efficiency is about $OE = 0.94$ (10.1), we obtain the result of [65] $\eta_{PV} = 0.13$. This is the true Shockley-Quesser limit for a flexible TFSC based on a-Si. And even this low limit is not approached in commercially available samples of flexible TFSCs. In 2009 commercially available TFSCs with a micron-thick PV layer and SiN antireflector on top of the front electrode demonstrated the same daytime-averaged overall efficiency about 3% as the TFSCs with the optimized thickness of the p-i-n structure [67]. In 6 years this value increased to $4-5\%$ [12]. So, in spite of the low efficiency, such advantages as low costs, light weight and flexibility determined fast development of thin-film solar photovoltaics in the past decade. Fifteen years ago flexible TFSCs based on a-Si had the cost 20 times lower than that of silicon solar cells, whereas their overall efficiency was lower only 5 times [20]. The overall comparison was evidently in favor of a-Si TFSCs.

Six years ago TFSCs were on the peak of their development and represented a point of keenest interest for both industry and research institutes. However, in 2013-2014 the situation dramatically changed. During these years the price of mono-crystalline silicon dropped several times and became comparable with the price of the other components of wafer solar panels. This development resulted from the ramp-up in the production of semiconductor devices for consumer electronics. In 2011-2012 the industry started to prepare large-area silicon crystals from waste accompanying fabrication of cell phones, tablets, and other widespread gadgets. Crystallization of the melt

waste did not imply an additional purification of Si. Fabrication of c-Si solar panels reduced the amount of industrial waste and became as nature-friendly as the production of a-Si TFSCs.

At the same time, the cost of a-Si also reduced similarly and became smaller than the cost of all other components of a thin-film panel. However, the cost of these components – anti-reflective coating, current-collecting electrodes, metal contacts, circuitry for matching the solar panel to the external load – kept the same. Therefore, the difference in prices per unit area of a monolithic SC based on c-Si and a TFSC based on a-Si has drastically changed in favor of c-Si. This change resulted in a crash of companies specializing in thin-film solar photovoltaics, and it appears that no one of them survived in 2015. Consequently, the amount of funds allocated for research in this area over the world squeezed several times [12]. Note, that this situation was predicted in 2011 in work [68]. In this report, researchers working in American solar power industry explained (properly but in vain) to their managers how to avoid the collapse of thin-film solar photovoltaics.

Let us briefly summarize their speculations. The industrial collapse of TFSCs does not mean that we should stop scientific research in this field. "Energy is needed where it is consumed" and this paradigm acts in favor of future TFSCs. The area of applicability of TFSCs is much wider than that of the silicon solar photovoltaics oriented to power plants. The main issue is the low efficiency of TFSCs that for flexible a-Si SCs fabricated by scientific groups as a rule does not exceed 5%, and this is so mainly due to low optical efficiency [12]. The market of TFSCs is waiting a pulse from a scientific breakthrough – a drastic enhancement of the optical efficiency of TFSCs without a significant increase of their costs is needed. Below we will show how this breakthrough may start.

10.5.2 ARC of nanospheres for a-Si solar cells and the issue of transmission losses

Although moth-eye ARCs are relatively inexpensive on condition of their mass production, they are considered by many authors as not affordable for TFSCs based on a-Si whose idea is a cheap electricity from flexible sheets. Therefore, alternative technical solutions for all-angle ARCs have been suggested for these TFSCs whose operation is presumably similar to that of moth-eyes. For example, one can take a honeycomb planar array of sil-
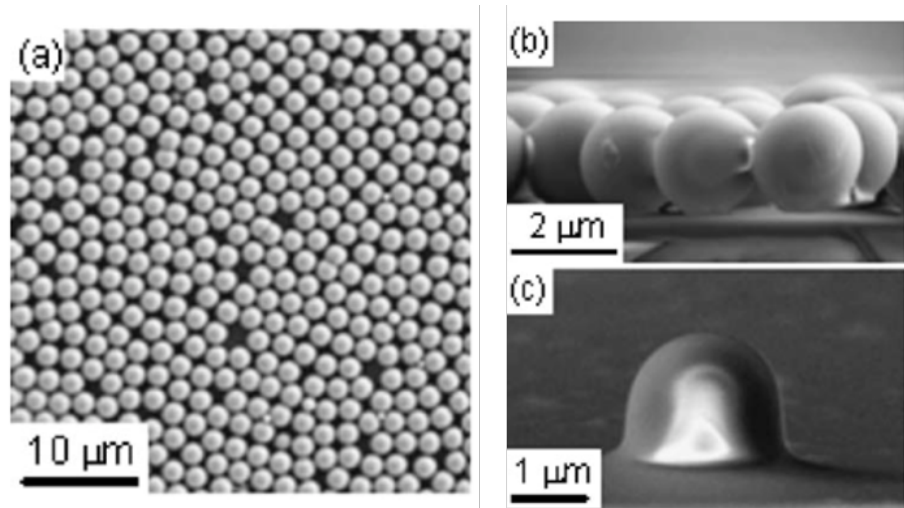
Figure 10.11: (a) Top view of an ARC of silica microspheres. (b) A SEM picture of the array in the vertical cross section. (c) A single microsphere encapsulated by a nanolayer of the spin-on glass illustrates the idea of a gluing laminate protecting the depicted nanostructure from abrasion and ensuring its mechanical robustness. Reproduced from [64] with permission of AIP Publishing.

ica spheres with the diameter 2 μm densely packed on the substrate and laminated by a glue of liquid glass, which was suggested in aforementioned work [64]. This monolayer is obtained using self-assembly, and its fabrication is even cheaper than the nanoimprint lithography used for moth-eye ARCs. Instead of c-Si as in [64] these microspheres can be placed on the surface of the top electrode of a TFSC (a TCO nanolayer). Well, the period of this array is optically large and in the reflected field the Fraunhofer diffraction lobes arise. However, the same technique can be used with smaller spheres. Detailed and accurate studies have shown that the best suppression of reflection for such an ARC located on top of a TCO layer (top electrode) of an amorphous-silicon TFSC and even of a gallium-arsenide SC is granted by submicron spheres [69–71].

As it was shown in [70–72], the operation of the ARC on top of a TFSC is similar to that of a flat multilayer ARC. For TFSCs any possibility to reduce the fabrication costs is important, and the fact that one can fabricate a cheap analogue of multilayer ARCs (due to their high cost utilized only in
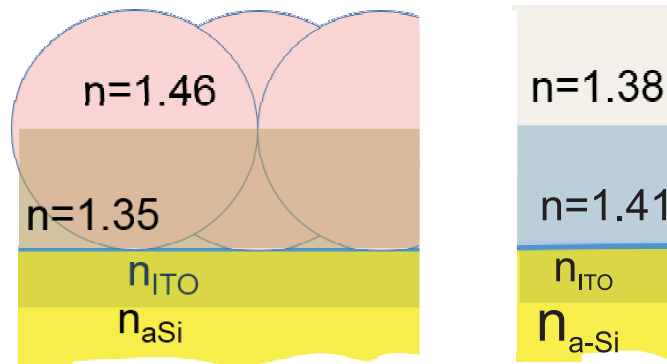
Figure 10.12: Multilayer model of the ARC of silica nanospheres of top of the a-Si TFSC. Left panel: the physical structure. Right panel: the model structure.

satellite SCs) was a great finding. A TFSC based on a-Si and enhanced by an optimal ARC of nanospheres comprise nanospheres of silica ($n_{sil} = 1.46$ in the visible range) with the diameter 700 nm fixed on top of the TCO by a 300 nm-thick layer of a polymer adhesive [73]. Its operation is qualitatively illustrated in Fig. 10.12 by an effective multilayer. This model is adequate for spheres with diameters smaller than $600 - 800$ nm [70–73]. Effectively, a PV layer with $n_{a-Si} \approx 3.2$ is covered by a layer of ITO with $n_{ITO} \approx 1.9$, covered in its turn by a composite layer with $n_1 = 1.41$ (silica and glue) and finally by a composite layer with $n_2 = 1.38$ (silica and air). The mean integral reflectance of such TFSC reduces to 11% compared to 23% corresponding to the bare TFSC. The mean integral optical loss in the 80-nm thick layer of ITO is 6%. Seemingly, this should have resulted in the daytime-averaged optical loss $OL = 17\%$. However, in reality the optical loss is much higher. In these estimates, we have neglected the optical loss in the back electrode where a substantial part of the incident light transmits.

Though the multilayer ARC in view of its low cost is excellent, and 83% of the solar power flux transmits into the PV layer, the optical loss is very high, $OL \approx 59\%$, whereas for a bare TFSC without any ARC we have $OL \approx 67\%$ [71]. The improvement granted to the optical efficiency by the ARC of silica spheres is too modest (8%) and hardly sufficient to justify even modest fabrication costs.

The p-i-n structure of the thickness $300 - 400$ nm is optically thin – it absorbs nearly one half of the solar power in one passage of the sunlight through

the layer. Another half of the power transmitted into the PV layer passes to the area of the back contact and is dissipated there. An ARC is not very useful – it replaces the reflection loss by the transmission loss. Transmission loss is the key issue for all flexible TFSCs, except aforementioned perovskite TFSCs (to be discussed separately).

Since an increase of the thickness of the PV layer compared to the optimal one results in the same reduction of the efficiency as the reduction of the transmission loss, the only remedy is trapping the sunlight inside the PV layer. To achieve this goal one should transform the incident plane waves into a package of such spatial harmonics which could stay inside the PV layer until the transmitted power is completely absorbed. It can be, for example, a package of evanescent waves – waves propagating in the horizontal direction and attenuating across the layer. It can be a package of Brillouin waves propagating in the PV layer like in a waveguide, or it can be any other waveform that would imply a better absorption of the solar energy inside the PV layer than that corresponding to a single plane wave propagating vertically (across the PV layer). This functionality is performed by specially engineered light-trapping structures.

10.5.3 Light trapping in epitaxial silicon solar cells

Historically first LTSs were engineered not for *flexible SCs* which on the microscopic level are flat multilayers, but for SCs based on epitaxial silicon. Epitaxial (polycrystal with submicron grains) silicon TFSCs were developed in 1970s in order to reduce the amount of purified silicon needed for producing usual silicon SCs in those old times.

The optimal thickness of a c-Si PV layer is within $200 - 300\,\mu$m. This interval of values expresses the trade-off between the mechanical robustness, necessity to minimize surface recombination, and maximal absorption of sunlight in the PV wafer. Meanwhile, the thickness of the PV layer of epitaxial Si cannot exceed $20\,\mu$m. The surface recombination for these SCs is not a key issue because the main PV conversion occurs in the p-doped layer sandwiched between heavily doped nanolayers (called $p+$ and $n+$ layers, respectively). In the epitaxial Si both diffusion length and mean free path of minor carriers are smaller than those parameters of c-Si by two orders of magnitude. The critical bulk recombination prohibits for these SCs a PV layer with a thickness $d > 20\,\mu$m. Moreover, if we ensure the maximal optical efficiency, it is better to reduce the thickness of the PV layer to $d = 200 - 400$ nm [19]. An

amazing economy of purified silicon and a similar reduction of fabrication waste made the epitaxial SCs very attractive for the industry in 1970s.

However, even the thickness of the PV layer $d = 2\ \mu$m was not sufficient for absorption of solar light during two passages through the layer. When such flat PV layers are backed by a polished metal electrode, nearly 20% of the power reflected by the bottom electrode transmits back to the air. If the electrode is not polished and represents a metal foil and a contact layer, even more power is absorbed in it. In both situations the ARC is not helpful at all because an ARC can prevent only the reflection from the top interface and can suppress neither the parasitic transmission of light downward nor backward transmission of light reflected from the bottom electrode. It is schematically shown in Fig. 10.13(a) for a bilayer ARC that practically eliminates reflectance for the normally incident light. On the photographic picture (top panel) this surface looks grey (not black) namely because it reflects a lot. Meanwhile, in 1970s SCs of epitaxial Si with $d = 200 - 400$ nm were developed whose overall efficiency without LTSs was very low. Therefore, already in 1970s the light-trapping research started in solar photovoltaics.

The most known technical solution (see e.g. in [75–77]) is the *pyramidal textures* – texturing of both top and bottom surfaces of the Si layer. The crystallography of Si allows such texturing with the pyramidal angle equal to 45°. On top of Fig. 10.13(b) an atomic-force microscope picture of such a surface is shown. The picture shows the domain beyond the microstrips of the grid electrode. Here, the averaged height of the pyramids is $1.5\,\mu$m. The textured surface is covered by an antireflector (75 nm of MgF) that also serves for passivation of polycrystalline Si reducing surface recombination. The physical mechanism of this LTS is illustrated by the sketch on the bottom panel. The texture diverts the rays of the sunlight and their oblique propagation in the PV layer makes the optical path of sunlight inside the PV layer sufficient for its full absorption. From the picture it is clear that this enhancement of the path length holds for any incidence angle. Only the rays incident to the pyramidal apex or to the crevice are scattered.

It is also clear that this explanation based on geometrical optics is restricted by diffraction effects. For an individual pyramid with the height larger than $1.5 - 2\,\mu$m in the range of the visible light these effects can be, in principle, negligible. However, the pyramidal texture of the top surface is obviously reproduced in the bottom surface of the PV layer – the substrate of polished silver that reflects the light [19, 20]. If the thickness of the PV layer is insufficient, the sunlight experiences strong diffraction on these two
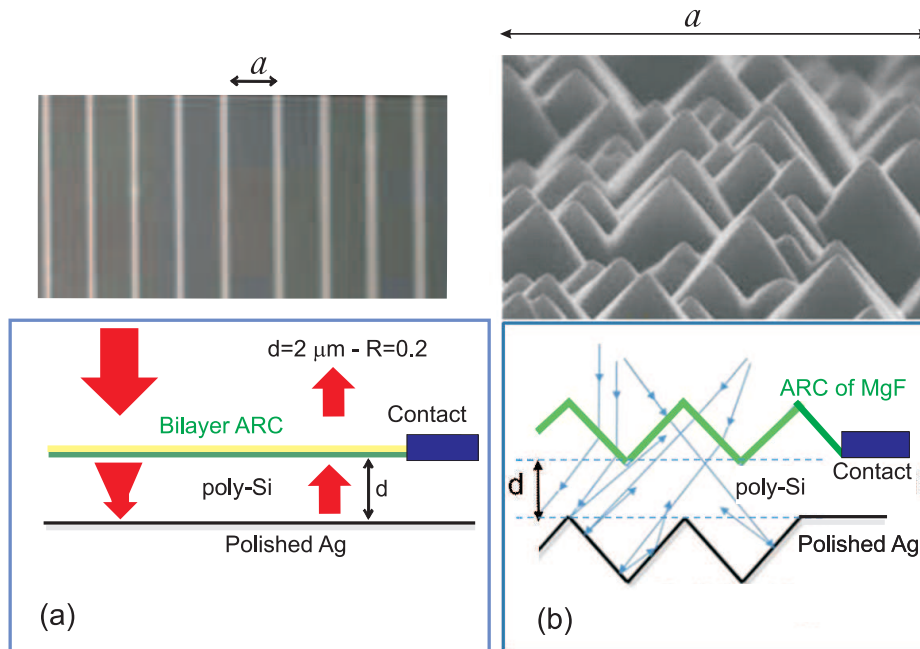
Figure 10.13: (a) Epitaxial-silicon SC of the thickness about $2\,\mu$m equipped with an optimal ARC (bottom panel) has the same reflective properties as the thick layer of silicon with the same contact mesh (top). (b) Pyramidal LTS for an epitaxial-silicon SC: sketch of the cross section illustrating the idea of the ray-type light trapping (bottom panel) and the AFM micrograph of the surface (top). Micrographs have been done by M. Omelyanovich.

parallel textures and the expectations about excellent light trapping and low scattering are not justified.

As it was shown in works [75–77], this ray light-trapping mechanism practically works only for $d > 1\,\mu$m. In fact, the condition of the applicability of the ray optics restricts also the minimal ratio d/h. First, the height h must be much larger than the effective wavelength in Si ($\lambda_{Si} = \lambda/n_{Si}$), second, the ratio d/h must be larger than unity [76]. Under these conditions, light trapping using pyramidal or conical textures may give enhancement of absorption in the PV layer (compared to the flat structure with the same thickness of all layers) up to $4n_{p-Si}^2$, where n_{p-Si} is the refractive index of the polycrystal Si. Of course, this ultimate gain can never be achieved, and this consideration only indicates huge potential of the light-trapping techniques.

For epitaxial TFSCs with $d < 1\,\mu$m *pyramidal textures* do not work, and for such TFSCs researchers have developed more sophisticated types of LTS, called photonic crystal LTSs (see e.g. [12]). Here, we do not discuss them, it is enough to mention that they are too expensive for commercialization. As to pyramidal textures, they have found application in wafer silicon solar cells as well due to their antireflective action for large incidence angles. Since such textures are covered by an antireflector of MgF, the Fraunhofer backscattering from them is weak. Except black-silicon SCs and SCs based on oxide tunneling junctions all silicon solar photovoltaics implies pyramidal texturing at least on top of the PV layer. Decrease of the mean integral reflectance granted by this texture is modest, but fabrication costs of the pyramidal texture are, nowadays, so low, that this modification is justified.

10.5.4 Plasmonic light trapping in thin-film solar cells

For amorphous silicon TFSCs pyramidal, conical or prismatic textures are not efficient because the PV layer is too thin. Moreover, this texturing technique is not compatible with the target of flexibility. For flexible TFSCs researchers have developed a lot of original LTSs. Most efforts of researchers were devoted to the development of so-called *plasmonic LTSs*. The history of this scientific direction started in 1990s by pioneering work [78] and since that time has resulted in hundreds if not thousands of journal papers reviewed in work [79]. This review, published in 2010, enthusiastically promoted the idea of plasmonic LTSs for amorphous solar photovoltaics. Meanwhile, work [80] (published also in 2010) criticized the whole approach because the light-trapping effect can be achieved only due to a plasmon resonance, obviously associated with resonant losses in the metal constituents of the LTS. Therefore the increase of the useful PV absorption due to subwavelength concentration of the field in the PV layer is obviously accompanied by an increase of the parasitic absorption. The discussion has continued since that time. Nowadays, the attitude of the solar photovoltaic community to plasmonic LTSs for amorphous TFSCs is controversial [12]. The question is especially keen due to the fact that in more than 20 years of its history, no one of hundreds plasmonic LTSs fabricated for amorphous-silicon TFSCs has been commercialized.

As a rule, plasmonic light-trapping implies subwavelength concentration of solar light transmitted into the PV layer. Due to the subwavelength size of plasmonic nanoparticles, this concentration is not light focusing – a process
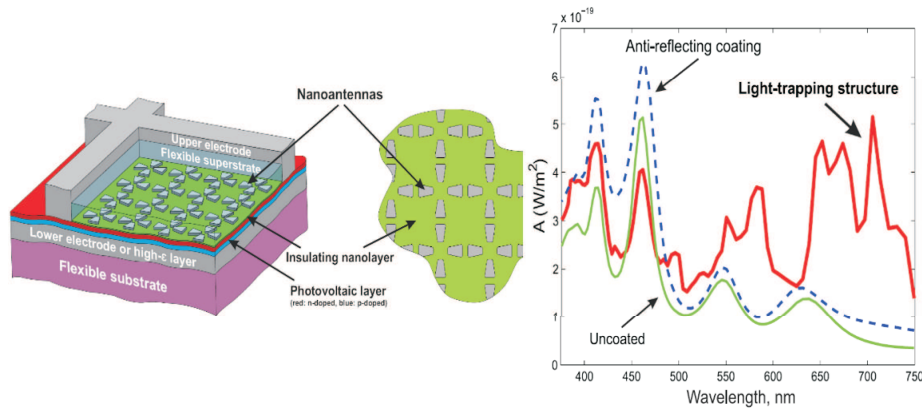
Figure 10.14: (a) Plasmonic LTS utilizing collective resonances of an array of specially designed nanoantennas. (b) Spectral absorption of sunlight for normal incidence calculated for a bare TFSC (based on a multicomponent semiconductor called CIGS), for the same TFSC with an antireflector, and for the same TFSC enhanced by a LTS. Reprinted from [96] with permission of Aalto University.

when the incident plane wave is converted into a beam of converging waves. It is conversion of the incident plane wave into a package of evanescent waves, exponentially decaying in the vertical direction. There is a point of view promoted and shared by many authors that simple ray focusing is unsuitable for TFSCs for two reasons. First, a converging light beam experiences the so-called free-space diffraction or *Abbe diffraction*. This effect restricts the applicability of the geometrical optics for the domain of the focal spot and restricts the minimal size of the focal spot by the value 1.22λ (calculated by Lord Rayleigh and called the *Rayleigh limit*). Most part of TFSCs have the PV layer of the thickness smaller than the minimal focal spot size, and, therefore, focusing is not a suitable mechanism for light trapping. Second, even for those TFSCs which have sufficient thickness of the PV layer, focusing is not suitable because it will reduce the current collection efficiency. A lens located on top of the TFSC will focus light in a micron-sized area of the PV layer. All the area of the SC around the focal spot will remain dark and the photocurrent will be not formed there. Thus, the effective area of the TFSC squeezes to the microscopic values and the output power will be small. Such light concentration would be reasonable only if the unit area of TFSC were much more expensive than the unit area of the lens. However,

the situation is the opposite. Solar light concentrators (Fresnel lenses and special mirrors) were strongly developed for solar photovoltaics 15–20 years ago (see e.g. in [20]) when wafer SCs were expensive and there was a market demand to decrease their area. Nowadays, silicon solar panels are cheaper than these lenses and mirrors, and TFSCs are much cheaper.

These authors conclude: Since the light focusing is not suitable for trapping light in a TFSC, one has to use nanostructured light concentrators, nearly uniformly covering the whole area of a TFSC [81–83]. The most suitable mechanism of such concentration appears to be the plasmon resonance (see similar speculations also in e.g. [84–86]). We may refer these plasmon resonances to two classes. The first class is that of localized surface plasmon resonances. These are resonances of an individual metal nanoparticle. In this book (Chapter 7) the dipole type of this resonance (that of a silver nanosphere) is analysed. Meanwhile, for substantial in size or complex-shaped particle of a plasmonic metal (usually Ag or Au) there are also multipole resonances, among them the most important for light trapping is the quadrupole one. The second class of plasmon resonances relevant for LTSs is represented by collective surface plasmon resonances – resonances of the whole nanostructure covering the area of the SC. These resonances result in formation of packages of surface waves called surface-plasmon polaritons.

Individual plasmon resonances can be engineered in rather cheap, chemically-manufactured plasmonic arrays called *metal island films*. A metal island film is an optically dense random array of Au or Ag nanoparticles with the typical sizes of the particles $20 - 200$ nm, whereas the dominant shape of the constitutive nanoparticles depending on the explicit technique can be different: from nanospheroids to nanopatches. As we have discussed in Chapter 9, too small nanoparticles manifest high losses and low magnitude of the plasmon resonance, thus particles smaller than 20 nm are not desirable. The maximal particle size is restricted by the requirement of low backscattering losses. The variation of the particle sizes and shapes offers overlapping plasmon resonances at different frequencies so that the resonance bands may cover an important part of the operation band of a TFSC (for those based on a-Si, up to one half of it [87, 88]).

However, broadband increase of absorption is not the only requirement for LTSs. The purpose of LTSs is broadband increase of the useful (PV) absorption and not the total absorption in the active layer into which the metal nanostructure is incorporated. However, many authors are happy to report the decrease of both integral reflectance and transmittances in the operation

band, meanwhile the optical loss in their structures is high due to the resonant dissipation in the metal nanoparticles [80]. Moreover, beyond the range of the consolidated plasmon resonance such LTSs increase the reflection loss (because a non-resonant metal structure creates a shadow behind it). This effect is not very significant if the metal island film is incorporated sufficiently deeply into the PV layer where the sunlight intensity already decays due to the PV absorption. However, such structures are more expensive than similar plasmonic LTSs located on top of the active layer. There were many attempts to suppress parasitic reflection from plasmonic island films located on top of a TFSC, such as the use of overlapping dipole and quadrupole plasmon resonances [89]. However, all these attempts resulted only in a small (narrow-band) enhancement. An efficient way to exploit localized surface plasmons in an LTS of a TFSC is to implement the bottom electrode of the SC as a metal island film located on a substrate of TCO [90, 91]. Then the light at frequencies beyond the plasmon resonance band is reflected into the PV layer. However, the hot spots resulting from the local field enhancement at the plasmon resonance still intersect with the metal nanoparticles.

Thus, it appears that cheap plasmonic nanostructures do not grant any significant improvement to any practical TFSC. Even in the case when gain in the PV absorption exceeds the increase of the parasitic absorption [90,91], the gain the overall efficiency it is not sufficient to justify the fabrication costs [12]. In fact, these costs are higher that initially expected because a metal island film incorporated into the PV layer or located on the back electrode surface needs to be isolated from the semiconductor. Otherwise the photoelectric conversion is spoiled by the atomic diffusion from the metal surface [92], and the gain in the optical efficiency is overcompensated by the decrease of internal quantum efficiency. In [12] it was concluded that all known attempts to enhance practical TFSCs using rather cheap, chemically manufactured plasmonic nanostructures have failed and the authors of [80] were right.

An alternative approach is exploitation of collective plasmon resonances which arise in periodic metal nanostructures. Utilizing collective plasmon resonances, one may minimize reflection losses, maximize the consolidated bandwidth of plasmon resonances and practically get rid of parasitic losses in metal elements, engineering evanescent wave packages so that the intensity maxima are located outside of metal. These advantageous operation regimes require a high regularity of metal elements dimensions and distances between them. Such elements prepared with nanometer precision are called *plasmonic*

nanoantennas [93–95]. Figure 10.14(a) shows an example of such LTS from [96]. This type of nanoantenna arrays is applicable to different types of flexible TFSCs from those based on a multicomponent semiconductor called CIGS [97] to a TFSC based on an organic PV material [98, 99]. Organic TFSCs do not refer to the class of PV diodes, they are called exitonic solar cells [98,99]. Nanoantennas depicted in Fig. 10.14(a) grant a drastic reduction of both reflection and transmission losses being located on top of the TFSC, and the additional absorption holds not in their metal elements. Comparison with the optimal ARC shows a noticeable enhancement in the integral PV absorption for all types of TFSCs studied in works [97–99]. The collective plasmon resonances exploited in these nanostructures were studied in work [100], where it was shown that these resonances form a consolidated resonance band suitable for light trapping. This band may occupy more than a half of the operation band of a SC. Figure 10.14(b) shows the spectrum of the PV (useful) absorption for three cases: bare SC, that enhanced by an ARC, and that enhanced by an LTS.

An array of nanoantennas can be fabricated also in the bottom part of the PV layer: at the interface with the bottom electrode. At the frequencies of the surface plasmon polariton resonances (which may occupy a significant portion of the operation band) an array of nanoantennas illuminated by a plane wave operates as a phase diffraction grating whose main diffraction maxima correspond to horizontally stretched wave vectors. The conversion of incident plane waves into such surface plasmon polaritons can be treated as conversion into waveguide modes propagating in the SC horizontally. The electric field of these modes almost does not penetrate into the back electrode (see e.g. in [101–104]).

However, the noticeable enhancement of the PV absorption (from 30% measured in [99] to 40% measured in [104]) accompanied by a corresponding enhancement of the overall efficiency from 18% (for organic solar photovoltaics in [99]) to 27% (for amorphous silicon solar photovoltaics in [104]) is not revolutionary. Recall, that the usual overall efficiency of a flexible TFSC based on a-Si is about 5% and the efficiency of a flexible organic SC is even lower. If we increase it up to 6.5% as in [104], it is not sufficient to justify the high fabrication cost of a regular plasmonic structure. When the back electrode is performed of polished silver and light can be absorbed after two passages through the PV layer, the optical efficiency is much higher and may attain 70%, whereas the light-trapping effect is wide-angle and broadband [102, 103]. Polished silver forms a good electric contact with the

amorphous silicon and there is no need in conductive paste. Unlike Al foils, silver polished with submicron precision does not imply parasitic light absorption in the contact domain. Therefore, nowadays such TFSC enhanced by a moth-eye ARC or an ARC of nanospheres can have $\eta = 11.3 - 11.5\%$ approaching to their Shockley-Queisser limit of 13% [65, 74]. However, such TFSCs are hard and have no perspective for civil terrestrial applications. They may find applications in space technologies where TFSCs can be preferred to multijunction SCs due to their incomparably lower mass per unit area [20].

Returning to flexible TFSCs, we have to state that although regular LTSs are efficient optically, they are very inefficient economically. Even if the nanoimprint lithography is involved as it was suggested in [96, 97], it is combined with preparation of golden nanoparticles using some physical techniques. Fabricated of a metallic nanostructure with a nanometer precision in large areas is, nowadays, a rather expensive process. Therefore, TFSCs whose LTSs exploit collective plasmon resonances can be made flexible, but can find only some restricted applications beyond mass production.

To conclude this discussion, one can assert that plasmonic LTSs for TF-SCs, in spite of the huge body of literature, are either inefficient or very expensive. Therefore, they do not promise a revival of the flexible TFSCs for commercial solar photovoltaics.

10.5.5   Dielectric light-trapping for amorphous-silicon solar cells

The general advantage of dielectric LTSs compared to metal ones is the practical absence of optical losses. Recall that the same consideration is the main motivation behind development of all-dielectric metasurfaces (Chapter 4). Of course, even transparent dielectric materials are not ideally transparent: The imaginary part of the complex permittivity is nonzero, but for many solid dielectrics this value is practically negligible in the optical range. There is a straightforward way for engineering all-dielectric LTSs. It is transformation of a previously known ARC dedicated to TFSCs (an affordable large-area nanostructure) into an LTS. For example, it is possible to trap light with a monolayer of silica nanospheres discussed above. To realize light trapping we should properly tune their diameter. In work [73] the light-trapping operation was noticed for nanospheres of diameter 700 nm. However, the mechanisms

of light-trapping in the densely-packed arrays of dielectric spheres can be different and the dominant mechanism depends on the sphere diameter (for a given refractive index). The mechanism of light trapping in [73] corresponding to the increase of the sphere diameter from 500 nm (the best ARC) to 700 nm (ARC with light-trapping functionality) was related to the *whispering gallery resonances* which arise in substantial in size dielectric cavities. However, this mechanism is not optimal for a LTS dedicated to amorphous silicon TFSCs. For example, in [73] the corresponding effect resulted in a very slight decrease of the transmission loss accompanied by 3% enhancement of useful absorption.

In works [105, 106] the authors suggested to transform an ARC of paper [64] into an LTS via a simple increase of the diameter of the spheres from 500 nm (optimal for antireflective operation) to 700 (see in [105]) or 900 nm (see in [106]). This modification increases the period of spherical particles. It exceeds the wavelength and the effect of the diffraction grid arises. Consequently, scattering back into air increases due to appearing diffraction lobes. However, the increase of the reflection loss (compared to the ARC of 500 nm large spheres) is small (about 10% for the integral reflectance) because the optical contrast of silica ($n_{silica} = 1.5$) and air is not very high. This increase is overcompensated by the significant light-trapping effect – reduction of the integral parasitic transmission by 18%. Thus, the gain in the PV absorption equals 8%.

When the diameter of silica spheres in the ARC of [64] is equal to 700 nm, the mechanism of light trapping is related to the generation of *whispering-gallery modes* in the spherical cavity [105]. In the absence of a substrate, these modes are practically not excited by the incident wave. In the presence of the substrate, the eigenmodes of the cavity are coupled to the substrate via near fields. In the corresponding frequency range this coupling gives rise to a whispering-gallery mode representing a set of intensity maxima (hot spots) and minima alternating around the cavity. The lowest hot spot extends outside the cavity and partially intersects with the substrate. The presence of other (unnecessary) hot spots inside the cavity does not result in a noticeable increase of parasitic absorption, because the cavity is practically lossless. Notice, that the bottom hot spot extends into the PV layer through the nanolayer of TCO. The field concentration results in both increased parasitic absorption and PV absorption, whereas the last one prevails (since the absorption of the PV material is much higher). Within the operation band of a TFSC based on a-Si a spherical cavity of silica with the diameter

700 nm has three whispering-gallery resonances. These resonances result in the relative bandwidth of the consolidated resonance band nearly equal to 10% [105]. The combination of this light-trapping effect with the antireflective properties of the LTS results in an increase of the overall efficiency of a flexible TFSC compared to the case when the monolayer of 500 nm-large spheres is used [105]. Though the self-assembly technique is, in principle, affordable for preparing large-area nanostructures, the resonant regime demands nanometer precision for the nanospheres. Therefore, it is difficult to judge does the 8% gain in the optical efficiency claimed in [105] justify the corresponding fabrication costs.

In [106, 107] another mechanism of light trapping by silica spheres was suggested and exploited. This is formation of a so-called photonic nanojet [108–112]. Roughly speaking, this effect means focusing of the incident plane wave into an elongated focal spot by a sphere whose radius is noticeably larger than the wavelength but still comparable with it. In the present case, it implies the spheres with diameters $D > 0.8\,\mu$m. The larger is the microlens, the thinner is the spot whose width can be estimated as $\lambda/2n$ (n is refractive index of the medium where the photonic nanojet propagates). A so thin focal spot is achieved when $D > 2\ \mu$m. An array of such microspheres produces a noticeable backscattering which overcompensates the gain granted by the reduction of transmission loss. However, for light trapping in practical TFSCs based on a-Si there is no need to enlarge the microspheres up to $D = 2\ \mu$m. Amorphous silicon is a highly refractive material, and even a microsphere with $D = 1\,\mu$m producing in the green range of the spectrum the focal spot of width $\lambda/n \approx 125$ nm (at $\lambda = 500$ nm $n \approx 4$) grants the field concentration sufficient for the complete absorption of sunlight in a layer $h = 330$ nm of intrinsic a-Si. An effective light beam incident on a sphere has the same diameter $D = 1\ \mu$m. This beam converts into a photonic nanojet whose diameter is 8 times smaller. It means the 64-fold increase of the light intensity inside the nanojet. In reality, this squeezing is not so spectacular, because the microsphere is not submerged into a-Si, it is located above it. In practice, the cross section of the wave beam shrinks at the wavelength 500 nm only 10 times. However, even this tenfold increase of the light intensity is enough so that to increase the absorption sufficiently and the parasitic transmission in a practical TFSC turns suppressed.

It is worth to stress that the formation of the photonic nanojet is a kind of focusing – it is not a subwavelength light concentration granted by a localized surface plasmon or a Mie resonance. The non-resonant nature of the
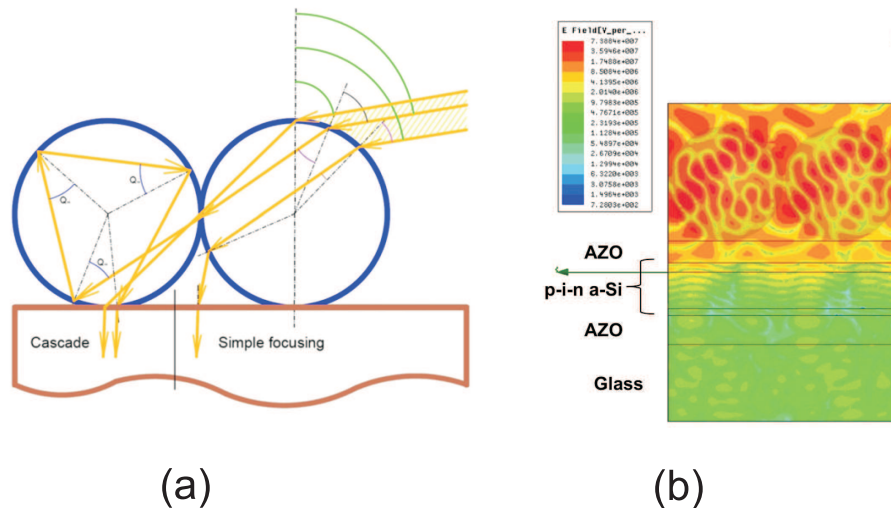
Figure 10.15: . (a) Schematics of the simple and cascade focusing of an obliquely incident light beam illuminating a reference sphere. (b) Color map of the electric field simulated for the case $\theta = 60°$. Simulations are performed by M. Omelyanovich.

phenomenon is its advantage. A sphere whose diameter D is chosen as a compromise between the minimization of the reflection (backscattering) loss and that of the transmission loss grants the sufficient gain for the PV absorption in the whole operation band of an a-Si SC. For the normal incidence this optimum corresponds to $D = 900$ nm [106]. The corresponding diffraction-limited light concentration is sufficient for practical absence of transmission loss. A more detailed analysis involving all angles of incidence typical for the daytime resulted in the optimal value $D = 1\,\mu m$ [107].

In fact, the advantage of this LTS compared to a simple antireflector arises only if we average the optical efficiency over all incidence angles corresponding to the daytime. Though for the normal incidence the parasitic transmission is prevented and the reflection loss is reduced as well, a simple focusing has a drawback discussed above. Namely, the photocurrent is generated only within the area of photonic nanojets. The PV layer beyond the nanojets remains dark. Therefore, the gain of enhanced PV absorption turns compensated by the decrease of the effective area of the SC. Fortunately, it is so only for the normal incidence. For obliquely incident waves the effective area of the SC suffers not so significantly. The solar flux obliquely impinging

one silica sphere of the array splits inside it onto two wave beams shown in Fig. 10.15(a). One wave beam (the lower ray) leaves from the sphere into the air gap (where it becomes a photonic nanojet) and transmits into the substrate. Another wave beam transmits to the adjacent sphere because the spheres in the array touch one another. In the adjacent sphere this second ray experiences three total internal reflections and finally transmits into the substrate in a different place. This mechanism of obtaining the second nanojet was called *cascade focusing*. In fact there are more than two rays because our sphere youches several neighbors. Numerical simulations illustrated by Fig. 10.15(b) confirmed the analytical model: we observed several light nanojets per unit sphere. As a result, the field concentration in the vertical direction prevails over the in-plane field concentration. For the angles larger than $40 - 45°$ almost the whole area of the PV layer is involved into generation of photocurrent and the parasitic transmittance keeps prevented like it is prevented for the normal incidence.

For the daytime-averaged overall efficiency this LTS grants the overall gain of 16% compared to the same TFSC covered by a simple antireflector of silicon nitride. The gain compared to the same TFSC enhanced by an ARC of nanospheres ($D = 500$ nm) is about 8%. A monolayer of densely packed micron-sized silica spheres operates as an efficient ARC for the reflected sunlight and as an efficient LTS for the transmitted sunlight [107]. Work [107] leaves no doubts which type of LTSs is more promising for amorphous silicon TFSCs (dielectric or plasmonic).

However, it is still not an optimal technical solution. Though the self-assembly allows manufacturing regular monolayers in large areas almost for free, this regularity holds only at the scale of a few millimetres. The defects in these monolayers are significant for practical samples – those having the sizes 3×3 cm or more. For such samples, regions where the monolayer is not formed cover nearly 20% of the area. In these regions, microspheres either form clusters (monolayer structures of $5 - 10$ densely packed spheres) or are isolated from one another by the micron gaps. The daytime-averaged integral reflectance of these defect areas is as high as 60-70% due to high back-scattering of microspheres. When only the defect areas are illuminated (by the collimated sunlight), the photocurrent per unit area turns twice as lower as that measured for a bare TFSC. The gain in the photocurrent per unit area reported in [107] referred to the special illumination. In this work, a collimated wave beam of millimeter width was directed to a regular part of the SC. For practical applications of a-Si TFSCs one should either eliminate

these defective domains from the samples (which is hardly affordable if this technical solution is commercialized) or somehow reduce the impact of defects to the optical efficiency of LTS.

10.5.6 Light-trapping structures integrated with the top electrode

A prototype of an affordable LTS in which the impact of defects is reduced can be also found among existing ARCs. In work [113] the authors revealed that nanopatterning of a flat antireflector by notches shaped as truncated cones improved its wide-angle operation. These notches of depths about 100 nm and width $200-300$ nm were prepared using nanoimprint lithography with the period $400-500$ nm in a layer of glass whose optimal thickness for antireflective operation on a-Si is about 110 nm. We have already seen that nanolithography is affordable for TFSCs being compatible with the roll-to-roll processing. Later, these ARCs were successfully applied for wide-angle suppression of reflection from optical glasses where similar notches were prepared in a polymer film of thickness 150 nm [114].

In work [115] light-trapping properties of similar notches when their horizontal sizes are increased up to 400 nm have been theoretically studied. Such notches still offer the antireflecting functionality but also enhance the local electric field, and the field concentration reduces parasitic transmittance through the PV layer of the TFSC. This effect is non-uniform over the visible range, as there are several local maxima. However, even at the minima the PV absorption is not worsened compared to that in the absence of dents. At the wavelength of 600 nm the collimated beam in a-Si has the characteristic width 300 nm, whereas the period of notches is 450 nm. In other words, the cross section of the wave beam illuminating one unit cell of the structure shrinks 2.25 times. This collimation was observed in simulations both in the contact layer of TCO and in the PV layer. Therefore, an array of dents promises an alternative technical solution to an array of spheres [115].

Later, it was realized that the focusing function of a truncated conical dent is weaker than that of a hemispherical dent of the same size. Also, it was found that the maximal increase of the PV absorption takes place when the dent depth (radius) is larger, namely for $r \approx 700$ nm (for air notches in silica). Larger radii than $r \approx 700$ nm are favourable for the light-trapping effect but imply an optically large period of the array and result in an increase
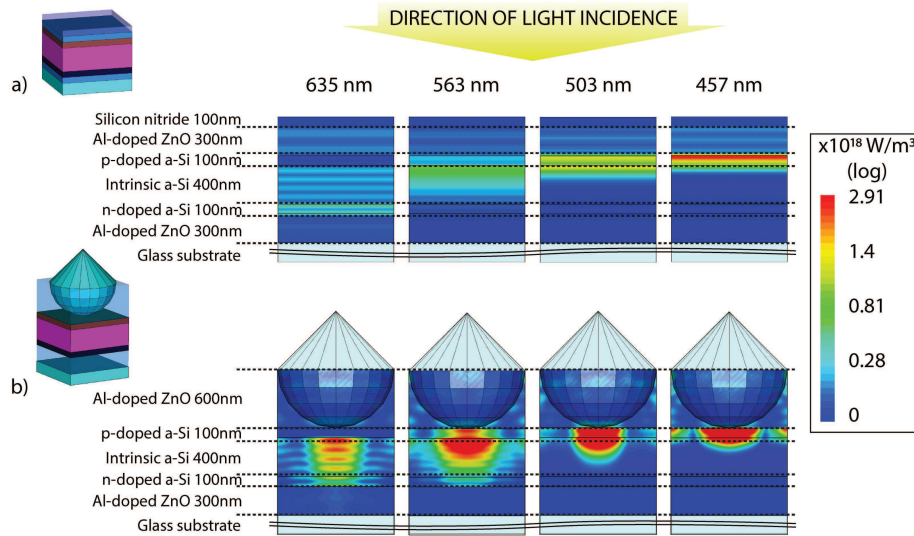
Figure 10.16: (a) Electric field intensity simulated for the reference structure with an ARC of SiN. (b) The same simulated for the structure with the LTS at four randomly chosen wavelengths. Simulations are done by M. Omelyanovich.

of reflection loss (as was discussed above). For the array of optimized notches formation of the collimated beam is observed in the whole visible range, as we can see in Fig. 10.16. It is analogous to the formation of a photonic nanojet: A hemispherical void cavity of micron diameter produces a photonic nanojet similarly to a dielectric microsphere.

Since the optimal dielectric antireflector is much thinner than the optimal notch depth, combining the light trapping and antireflective properties of such an array is problematic. A possible solution is using a densely-packed array of notches in the top electrode. In paper [116] it was a layer of AZO with the thickness $h = r = 600$ nm. The radius $r = 600$ nm is optimal for densely packed hemispherical voids in AZO (the period $1.2\,\mu$m). In this LTS each notch contains a semi-diamond particle of silica (i.e., a particle whose bottom half is a hemisphere and the top half is a cone). The optical contrast of AZO ($n_{\mathrm{AZO}} \approx 2$) with silica ($n_{\mathrm{sil.}} \approx 1.4$) is sufficient to realize the nanojet effect (for air notches the optimal radius is smaller). Meanwhile, the array of silica cones operates like a moth-eye ARC. In Fig. 10.16(a) we show the

intensity map of the electric field for the reference structure: the same TFSC enhanced by an antireflector of silicon nitride, and in Fig. 10.16(b) the map corresponds to the LTS described in paper [116]. Strong field concentration indicates the light-trapping effect in the whole visible range.

At a first glance, it seems that the fabrication of such light-trapping and antireflecting top electrode is difficult and expensive. However, it is not so. At the first step, a monolayer of colloidal silica microspheres is prepared using the self-assembly, The substrate to which the colloidal silica spheres attach from the colloidal suspension is p-doped a-Si. As a result, a monolayer of silica spheres is obtained on top of the PV layer of our SC before we have started the fabrication of the top electrode. On the next step, the textured electrode of AZO is fabricated using a machine for large-area atomic layer deposition. It produces a film centered by spherical voids of silica of radius r and thickness $h = 2r$ inside AZO. This process for the area $10\,cm^2$ is shorter than an hour.

At the last stage, the top half of this composite film is removed. This removal is done with the nanometer quality which is offered by the ion-beam etching (IBE) technique. This technique is much faster than the ion beam lithography utilizing nanofocused ion beams. Basically, the beam of Ar ions of a few nm thickness and macroscopic (millimeter scale!) length is an effective blade cutting solid dielectric or semiconductor surfaces at any angle up to the grazing one (as in our case). Such IBE process takes about 11 minutes for the area of 10 cm² and results in a regular arrangement of high-quality hemispherical cavities filled with semi-diamond silica microparticles. Surprisingly, the top half of a silica sphere is not removed but is transformed into a conical protrusion. These conical protrusions serve as an ARC of the SC.

Of course, self-assembly inevitably results in defect regions of nearly one millimetre size where the needed monolayer of spheres is not formed. In test samples of the size about 10 cm² these regions cover about 20% of the whole area. In these defect areas, we observe isolated nanocones and clusters of nanocones (few hundreds per square millimeter). However, these defect areas scatter much weaker than those in the earlier LTS. This is so because nanocones are not so efficient back-scatterers as microspheres. This experimental fact agrees with optical simulations. The angle-averaged integral reflectance of a defect region is nearly equal to that for a bare SC. Meanwhile, the areas with the regular arrangement of insertions offer a triple reduction of the averaged reflectance. Finally, in spite of the defect regions, the mean PV

absorption of such TFSC growth twice as compared to the same TFSC with a simple antireflector on top of a flat AZO layer. It is important to stress that this result was obtained illuminating the whole area of the SC [116]. The measured daytime-averaged optical efficiency of the SC is 60%. It is the best known result for flexible TFSCs up to now.

However, for commercialization of a new LTS, a demonstration of its high *optical* efficiency is not enough. The researchers have to experimentally demonstrate a record *overall* efficiency, obtained due to the new LTS. For the moment, in the literature there are data on several very efficient LTSs demonstrating enhancements close to that claimed in paper [116] (see e.g. [117–119]). However, record efficiencies of flexible TFSCs were not obtained in any of these works. It is not surprising, because experts in experimental nanophotonics are rarely capable of fabricating high-quality SCs. Vice versa, experts in experimental photovoltaics can rarely fabricate high-quality nanostructured LTSs and ARCs. Successful collaborations between these two scientific communities occurs seldom. When it occurs, results can be exciting: in work [120] such collaborative team has claimed a record for the mean overall efficiency of a flexible a-Si TFSC $\eta = 8.2\%$. The collaboration of nanophotonic and photovoltaic teams is a prerequisite for bringing the overall efficiency of flexible TFSCs to the Shockley-Queisser limit.

10.6   Conclusions

In this chapter we have discussed SCs of the so-called diode type and analyzed typical reasons for losses of sunlight power in them. We have analysed the role of the optical loss for the overall efficiency of the SCs and showed that optical nanostructures integrated with SCs can significantly decrease their effective (integral over the frequencies and averaged over the incidence angle) optical loss factor compared to the conventional flat structures. In our analysis we kept in mind commercialization readiness of all technical solutions that usually required nanotechnologies which would be affordable for large-area samples. We have shown that for thick SCs the best currently known technical solution is represented by black silicon for SCs based on c-Si and by moth-eye ARCs for some other types of SCs. However, for flexible TFSCs the promising approach is the replacement of a nanostructured ARC by a nanostructured LTS. We have shown that dielectric nanostructures and nanostructures combined with a transparent (semiconducting but not pho-

tovoltaic) electrode are much more promising for industrial adaptation than plasmonic LTSs, which are more popular among researchers.

Note, that in this book we did not consider nanostructures dedicated to reduction of intrinsic Losses 1–3, i.e., optimization of the optical absorption in the PV layer [12]). This task refers to solid-state physics. Also, we have not considered arrayed SCs consisting of PV nanoelements, such as resonant nanowires or nanospheres of PV materials which allow resonant optical absorption of sunlight in effective areas exceeding their physical size. We have not concerned many related questions on the edge between photonics and nanophotonics. For example, we have not discussed ARCs of dielectric nanospheres for GaAs SCs, which have no conventional counterparts (because dielectric layers as well as TCOs cannot attach to a flat surface of GaAs). We have not discussed the enhancement of SCs by the so-called hot electrons produced in plasmonic nanoparticles (see e.g. in [12]). So, we have omitted many issues related to nanostructures in SCs. Our first goal was to introduce the reader into the topic. Our second goal was to show how much work remains in the field of solar photovoltaics to a researcher working on the edge between nanophotonics and conventional photonics and electronics. We have done it on examples of available technical solutions.

Problems and control questions

1. Consider a simple antireflector: a layer of the dielectric medium with the refractive index n_A of thickness d sandwiched between two half-spaces: free space and a photovoltaic medium with the refractive index n_{PV}. Assume that the optical losses in media are negligibly small. Prove that at the wavelength λ_0 corresponding to $d = \lambda_0/4n_A$ the power reflectance R of the normally incident plane wave can strictly vanish. Find the relation between n_A and n_{PV} which offers this regime.

2. Calculate numerically the power reflectance R versus λ in the vicinity of the antireflective wavelength λ_0. Find the band in which $R < 0.1$ if $n_{PV} = 3.6$ (a good approximation for c-Si in the range $600 - 900$ nm).

3. Find the antireflective condition for an arbitrary incidence angle θ. Calculate numerically the power reflectance R versus λ and θ in the vicinity of the antireflective wavelength λ_0 and antireflective angle θ_0. Take, for example, $\lambda_0 = 600$ nm, $\theta_0 = 30°$, $n_{PV} = 3.6$. Find the band

of wavelengths and the sheer of angles in which $R < 0.1$ and depict this region in the coordinate frame (λ, θ).

4. Why the bandgap of the PV semiconductor cannot be chosen to make the spectral efficiency equal 100%?

5. Why the p-n junction is helpful for efficient conversion of light into electricity?

6. Why the Shockley-Queisser limit for silicon solar cells is as low as $\eta_{\max} = 1/3$ and cannot be beaten? List all the reasons you know.

7. What is the main reason why the Shockley-Queisser limit is not achieved even in advanced solar cells?

8. Multijunction (cascaded) solar cells allow one to beat the Shockley-Queisser limit for silicon solar cells because they split the solar spectrum onto several parts. Why this spectrum splitting increases the overall efficiency? Which type of loss is reduced in every cascade?

9. Why multilayer antireflective coatings are used in the satellite solar cells and not used in the commercial ones?

10. Destructive interference of two waves reflected from two interfaces is impossible for the front glass of a solar cell because the nanometer precision parallelism of two surfaces is impossible for a macroscopic layer. However, the front glass decreases the reflectance of a bare solar cell. Why?

11. Why the presence of a front glass erases the benefits granted by a multilayer antireflective coating compared to a simple antireflector?

12. Why a moth-eye antireflecting coating is more broadband than a simple antireflector?

13. Why a moth-eye antireflecting coating is more wide-angle than a simple antireflector?

14. Why black silicon is better for silicon solar cells than a moth-eye antireflecting coating?

15. What are advantages and drawbacks of thin-film solar photovoltaics compared to silicon one?

16. Explain why an array of silica nanospheres on top of an amorphous-silicon solar cell operates as a bilayer antireflective coating?

17. Which type of optical loss – reflection or transmission loss – is suppressed in the light-trapping structure performed as a pyramidal texture? What do you say about the second type of optical loss – does it keep the same level after this texturing or increases? If it increases, why?

18. What is the main drawback of plasmonic light trapping in the random metal nanostructures?

19. What is the main drawback of plasmonic light trapping structures performed as regular arrays?

20. Why all-dielectric light trapping is not very efficient if based on the cavity resonaances?

21. Why dielectric microspheres forming the nanojet operate better when are illuminated obliquely compared to their operation for normal incidence? Is this advantage better light trapping of the obliquely incident light or something else?

22. Why the dielectric light-trapping structure integrated with the top transparent electrode operates better than the monolayer of spheres? What is the advantage of conical protrusions?

Bibliography

[1] W. Palz, *Power for the World – Emergency of Electricity from the Sun*, Pan Stanford Publishing, Brussels (2010).

[2] E. Becquerel, Mémoire sur les effets électriques produits sous l'influence des rayons solaires, *Comptes Rendus* **IX**, 561–567 (1839).

[3] W.G. Adams and R.E. Day, The action of light on selenium, *Phil. Trans. Roy. Soc.* **167**, 313-349 (1877).

[4] C.E. Fritts, On a new form of selenium photocell, *American Journal of Science* **26**, 465-466 (1883).

[5] A. Stoletow, Suite des recherches actino-électriques, *Comptes Rendus* **CVII** 91-120 (1888).

[6] A. Einstein, Über einen die Erzeugung und Verwandlung des Lichtes betreffenden heuristischen Gesichtspunkt, *Annalen der Physik* **17**, 132-148 (1905).

[7] A. Fahrenbruch and R. Bube, *Fundamentals of solar cells: Photovoltaic solar energy conversion,* Academic Press, New York–London (1983).

[8] A. Luque and S. Hevedus, *Handbook of Photovoltaic Science and Engineering*, Wiley, NY (2002).

[9] W. Franz, Einfluss eines elektrischen Feldes auf eine optische Absorptionskante, *Zeit. Naturforschung* **13a**, 484–489 (1958).

[10] L.V. Keldysh, Behaviour of non-Metallic crystals in strong electric fields, *Soviet Physics JETP* **6**, 763–770 (1958).

[11] W. Shockley and H.J. Queisser, Detailed balance limit of efficiency of p-n junction solar cells, *J. Appl. Phys.* **32**, 510-519 (1961).

[12] V.A. Milichko, A.S. Shalin, I.S. Mukhin, A.E. Kovrov, A.A. Krasilin, A.V. Vinogradov, P.A. Belov and C.R. Simovski, Solar photovoltaics: modern state and trends, *Physics Uspekhi* **186**, 801-852 (2016).

[13] L. Zhu, A. Raman, K.X. Wang, M.A. Anoma, and S. Fan, Radiative cooling of solar cells, *Optica* **1**, 32-38 (2014).

[14] C. Liebert and R.R. Hibbard, *Theoretical temperatures of thin-film solar cels in Earth orbit*, NASA Technical Note D-4331, Nat. Aeronaut. Space Admin., WA (1968).

[15] S.H. Glick, F.J. Pern, D. Tomek, J. Raaff, and G.L. Watson, Performance degradation of encapsulated monocrystalline Si solar cells upon

accelerated weathering exposures, *Proc. NCPV Program Review Meeting*, Lakewood, Colorado, 14-17 October 2001, paper NREL/CP-520-30841. Available at http://www.osti.gov/bridge.

[16] N.-G. Park, Perovskite solar cells: an emerging photovoltaic technology, *Materials Today* **19**, 65-72 (2015).

[17] A.K. Chilvery, A.K. Batra, B. Yang, K. Xiao, P. Guggill, M.D. Aggarwal, R. Surabhi, R.B. La, J.R. Currie, and B.G. Penn, Perovskites: transforming photovoltaics, a mini-review, *J. Photonics for Energy* **5**, 057402 (2015).

[18] M. Stolterfoht, C.M. Wolff, Y. Amir, A. Paulke, L. Perdigo N-Toro, P. Caprioglio, and D. Nehe, Approaching the fill factor Shockley–Queisser limit in stable, dopant-free triple cation perovskite solar cells, *Energy Environ. Sci.* **10**, 1530-1539 (2017).

[19] Y. Hamakawa, *Thin-film solar cells: Next generation photovoltaics and its applications*, Springer, Berlin-New York (2004).

[20] A. Marti and A. Luque, *Next-generation photovoltaics*, IoP Publishing, London (2004).

[21] M.A. Green, The path to 25% silicon solar cell efficiency: history of silicon cell evolution, *Prog. Photovoltaics: Res. Appl.* **17**, 183–189 (2009).

[22] K. Yoshikawa, H. Kawasaki, W. Yoshida, T. Irie, K. Konishi, K. Nakano, T. Uto, D. Adachi, M. Kanematsu, H. Uzu and K. Yamamoto, Silicon heterojunction solar cell with interdigitated back contacts for a photoconversion efficiency over 26% Nature Energy 2, 17032 (2017).

[23] M.A. Green, *Third-generation photovoltaics*, Springer, Berlin (2004).

[24] G.K. Dey and K.T. Ahmed, Performance characterization of photovoltaic technology with highly efficient multi-junction solar cells for space solar power satellite systems *Proc. 3d International Conference on Green Energy, Green Engineering and Technology*, Dhaka, Bangladesh, Sep. 11-12, 2015, pp. 1-6.

[25] C.S. Fueller and G.L. Pearson, A new silicon p-n junction photocell for converting solar light to electricity, *J. Appl. Phys.* **25**, 676-677 (1954).

[26] J.A. Kong, *Theory of Electromagnetic Waves*, Wiley, NY (1975).

[27] A. Osipov and S. Tretyakov, *Modern Electromagnetic Scattering Theory with Applications*, Chichester, UK: John Wiley & Sons (2017).

[28] H.A. Macleod, *Thin Film Optical Filters* (3rd ed.), IOP Publishing London (2001).

[29] H.K. Raut, V.A. Ganesh, A.S. Nair, S. Ramakrishna, Anti-reflective coatings: A critical, in-depth review, *Energy Environ. Science* **4**, 3779-3804 (2011).

[30] M.A. Kats, R. Blanchard, P. Genevet, and F. Capasso, Nanometer-scale optical coatings based on strong interference effects in highly absorbing media, *Nat. Mater.* **12**, 20–24 (2013).

[31] J. Zhao and M.A. Green, Optimized antireflection coatings for high-efficiency silicon solar cells, *IEEE Trans. Electron. Dev.* **38**, 1925-1934 (1991).

[32] B. Thaidigsmann, E. Lohmuller, U. Jager, S. Mack, F. Lottspeich, A. Spribille, K. Birmann, D. Erath, A. Wolf, F. Clement, D. Biro, R. Preu. Large-area p-type HIPMWT silicon solar cells with screen printed contacts exceeding 20% efficiency, *Physica Status Solidi Rapid Research Letters* **5**, 286–288 (2011).

[33] K. Nurrows and V. Fthenakis, Glass needs for a growing photovoltaic industry, *Solar Energy Materials and Solar Cells* **132**, 455-459 (2015).

[34] P.B. Clapham and M.C. Hutley, Reduction of lens reflection by moth-eye principle, *Nature***244**, 281–282 (1973).

[35] V. Hotar, O. Matusek, and J. Svoboda, Laboratory detection of flat glass shapes using its reflection, *MATEC Web of Conferences* **89**, 01007 (2017).

[36] A. Parretta, A. Sarno, P. Tortora, H. Yakubu, P. Maddalena, J. Zhao and A. Wang, Angle-dependent reflectance measurements on photovoltaic materials and solar cells, *Optics Comm.* **172**, 139-151 (1999).

[37] Q. Chen, G. Hubbard, P.A. Shields, C. Liu, D.W.E. Allsopp, W.N. Wang, and S. Abbott, Broadband moth-eye antireflection coatings fabricated by low-cost nanoimprinting, *Applied Physics Letters 94*, 263118 (2009).

[38] N. Yamada, T. Ijiro, E. Okamoto, K. Hayashi, and H. Masuda, Characterization of antireflection moth-eye film on crystalline silicon photovoltaic module, *Opt. Express* **19**, A118–A125 (2011).

[39] S.A. Boden and D.M. Bagnall, Optimization of moth-eye antireflection schemes for silicon solar cells, *Prog. Photovolt: Res. Appl.* **18**, 195–203 (2010).

[40] J. Tommila, A. Aho, A. Tukiainen, Ville Polojärvi, Joel Salmi, Tapio Niemi, and Mircea Guina, Moth-eye antireflection coating fabricated by nanoimprint lithography on 1 eV dilute nitride solar cell, *Progr. Photov.: Res. Applic.* **21**, 1158-1162 (2012).

[41] K.-S. Han, J.-H. Shin, W-Y. Yoon, and H. Lee, Enhanced performance of solar cells with anti-reflection layer fabricated by nano-imprint lithography, *Solar Energy Materials and Solar Cells* **95**, 288-291 (2011).

[42] L.W. Chan, D.E. Morse, and M.J. Gordon, Moth-eye-inspired antireflective surfaces for improved IR optical systems and visible LEDs fabricated with colloidal lithography and etching, *Bioinspiration and Biomimetics* **13** 041001 (2018).

[43] A. Scheydecker, A. Goetzinger and V. Wittner, Reduction of reflection losses of PV-modules by structured surfaces, *Solar Energy* **53**, 171-176 (1994).

[44] C. Ballif, J. Decker, D. Borchert, and T. Hofmann, Solar glass with industrial porous SiO2 antireflection coating: Measurements of photovoltaic module properties improvement and modelling of yearly energy yield gain, *Solar Energy Materials and Solar Cells* **82** 331-344 (2004).

[45] P.G. Carey, J.B. Thompson, and R.C. Aceves, Solar cell module lamination process, US Patent No 6,340,403 B1, issued Jan. 22, 2002.

[46] X. Liu, P. Coxon, and M. Peters, Black silicon: fabrication methods, properties and solar energy applications, *Energy Environ. Science* **7**, 3223-3230 (2014).

[47] P. Repo, A. Haarahiltunen, L. Sainiemi, M. Ylikoski, H. Talvitie, M Schubert, and H.Savin, Effective passivation of black silicon surfaces by atomic layer deposition, *IEEE J. Photovoltaics* **3**, 90-94 (2012).

[48] H. Savin, P. Repo, G. von Gastrow, P. Ortega, E. Calle, M. Garin and R. Alcubilla, Black silicon solar cells with interdigitated back-contacts achieve 22.1% efficiency, *Nat. Nanotech.* **10**, 624-628 (2015).

[49] Z.-Q. Zhou, F. Hu, W.-L. Zhou, H.-Ya. Chen, L. Ma, C. Zhang, and M. Li, An Investigation on a crystalline-silicon solar cell with black silicon layer at the rear, *Nanoscale Res. Lett.* **12**, 623-626 (2017).

[50] Y.-J. Hung, S.-L. Lee, and L.A. Coldren, Deep and tapered silicon photonic crystals for achieving anti-reflection and enhanced absorption, Opt. Express 18, 6841-6852 (2010).

[51] J. Lv, T. Zhang, P. Zhang, Y. Zhao, and S. Li, Review application of nanostructured black silicon, *Nanoscale Res. Lett.* **13**, 110 (2018).

[52] T. Zhang, P. Zhang, S. Li, W. Li, Z. Wu and Y. Jiang, Black silicon with self-cleaning surface prepared by wetting processes, *Nanoscale Research Lett.* **8**, 351 (2013).

[53] M. Osborne, Hevel achieves heterojunction cells with 22.8% efficiency as plant ramps, PV-Tech, Jan. 29, 2018, available at https://www.pv-tech.org/news/hevel-achieves-heterojunction-cells-with-22.8-efficiency-as-plant-ramps.

[54] D. Andronikov, A. Abramov, S. Abolmasov, K. Emtsev, G. Ivanov, I. Nyapshaev, D. Orekhov, A.V. Semenov, G. Shelopin, E. Terukova, E.I. Terukov and A. Titov, A successful conversion of silicon thin-film solar module production to high efficiency heterojunction technology, *Proc. European PV Solar Energy Conference EU PVSEC'2017*, Sep. 24-28, 2017, Brussels, Belgium, Paper 2AV.3.12.

[55] M. Petrov, K. Lovchinov, M. Mews, C. Leendertz and D. Dimova-Malinovska, Optical and structural properties of electrochemically deposited ZnO nanorod arrays suitable for improvement of the light harvesting in thin film solar cells, *Journal of Physics: Conference Series* **559**, 012018 (2014).

[56] S. Abolmasov, P. Roca-i-Cabarrocas, and P. Chatterjee, Towards 12% stabilised efficiency in single junction polymorphous silicon solar cells: experimental developments and model predictions, *European Physical Journal: Photovoltaics* **7**, 70302 (2016).

[57] M.R. Maghami, H. Hizam, C. Gomes, M.A. Radzi, M.I. Rezadad, and S. Hajighorbani, Power loss due to soiling on solar panel: A review, *Renew. Sustain. Energy Rev.* **59**, 1307-1316 (2016).

[58] A.B. Roy, A. Dhar, M. Choudhuri, S. Das, S.M. Hossain and A. Kundu, Black silicon solar cell: analysis optimization and evolution towards a thinner and flexible future, *Nanotechnology* **27**, 305302 (2016).

[59] E. Ogorodnikov, In the scattered Light of the Russian sun, *RusNano News*, Sep. 11 (2017), available at http://en.rusnano.com/press-centre/media/20170911-expert-in-the-scattered-light-of-the-russian-sun.

[60] V. Vavilov, R. Aflyatonov, and A. Yakupov, Usage of the solar radiation potential in the republic of Bashkortostan of Russian Federation, *Proc. 2nd International Conference on Industrial Engineering, Applications and Manufacturing ICIEAM'2016* May 19-20, Chelyabinsk, Russia, 2016, Pages 1-5.

[61] J.B. Heng, C. Yu, Z. Xu and J. Fu, Solar cell with oxide tunneling junctions, Patent US2011/0272012A1, issued on Oct. 11, 2011.

[62] J.B. Heng, J. Fu, Z. Xu and Z. Xie, Back junction solar cell with tunnel oxide, Patent US2012/0318340A1, issued on Dec. 20, 2012.

[63] J. Fu, J.B. Heng, C. Yu, Tunneling-junction solar cell with copper grid for concentrated photovoltaic application, Patent US2015/0236177A1, issued on Aug. 20, 2015.

[64] M. Tao, W. Zhou, H. Yang, and L. Chen, Surface texturing by solution deposition for omnidirectional antireflection, *Appl. Phys. Lett.* **91**, 081118-1-081118-3 (2007).

[65] W. Qarony, M.I.Hossain, M.K. Hossain, M.J. Uddin, A. Haque, A.R. Saad, and Y.H. Tsang, Efficient amorphous silicon solar cells: characterization, optimization, and optical loss analysis, *Results in Physics* **7**, 4287-4293 (2017).

[66] A. Alkaya, R. Kaplan, H. Canbola, and S.S. Hegedus, A comparison of fill factor and recombination losses in amorphous silicon solar cells on ZnO and SnO2, *Renewable Energy* **34**, 1595-1599 (2009).

[67] *Ultra-Low-Cost Solar Electricity Cells, An Overview of Nanosolar's Cell Technology Platform*, Nanosolar Inc. White Paper (2009), available at
www.catharinafonds.nl/wp-content/uploads/2010/03/NanosolarCellWhitePaper.pdf.

[68] *U.S. Solar Market Insight Report*, Solar Energy Industries Association Year-in-Review (2011).

[69] T.-H. Chang, P.-H. Wu, S.-H. Chen, C.-H. Chan, C.-C. Lee, C.-C. Chen and Y.-K. Su, Efficiency enhancement in GaAs solar cells using self-assembled microspheres, *Optics Express* **8**, 6519-6524 (2009).

[70] J. Grandidier, D. M. Callahan, J. N. Munday, and H. A. Atwater, Configuration optimization of a nanosphere array on top of a thin-film solar cell, *Adv. Mater.* **32**, 1272–1276 (2011).

[71] A.S. Shalin and S.A. Nikitov, Approximate model for universal broadband antireflection nano-structure, *Progress in Electromagnetic Research B* **47**, 127-144 (2013).

[72] S. Dias, C. Banerjee, and A. Kundu, Silica nanoparticles on front glass for efficiency enhancement in superstrate-type amorphous silicon solar cells, *J. Physics D: Applied Physics* **46**, 415102 (2013).

[73] J. Grandidier, D.M. Callahan, J.N. Munday, and H.A. Atwater, Light absorption enhancement in thin-film solar cells using whispering gallery modes in dielectric nanospheres, *Advanced Materials* **23**, 1272-1276 (2011).

[74] T. Matsui, H. Sai, K. Saito, and M. Kondo, High-efficiency thin-film silicon solar cells with improved light-soaking stability, *Proc. 27-th Int. Conf. Progress in Photovoltaics*, Frankfurt, Germany p. 2213-2217 (2013).

[75] E. Yablonovitch, Intensity enhancement in textured optical sheets for solar cells, *IEEE Trans. Electron. Dev.* **29**, 300-308 (1982).

[76] P. Campbell, Light trapping in textured solar cells, *Solar Energy Materials* **21**, 165–172 (1990).

[77] Z. Yu, A. Raman, S. Fan, Fundamental limit of light trapping in grating structures, *Opt. Express* **18**, A366-A380 (2010).

[78] H.R. Stuart and D.G. Hall, Absorption enhancement in silicon-on-insulator waveguides using metal island films, *Applied Phys. Lett.* **69**, 2327-2340 (1996).

[79] H.A. Atwater and A. Polman, Plasmonics for improved photovoltaic devices, *Nature Mat.* **9**, 205-209 (2010).

[80] Yu. A. Akimov, W. S. Koh, S.Y. Sian, and S. Ren, Nanoparticle-enhanced thin-film solar cells: metallic or dielectric nanoparticles? *Appl. Phys. Lett.* **96**, 073111 (2010).

[81] P. Spinelli, V.E. Ferry, J. van de Groep, M. van Lare, M.A. Verschuuren, R.E.I. Schropp, H.A. Atwater and A. Polman, Plasmonic light trapping in thin-film Si solar cells, *J. Opt.* **14**, 024002 (2012).

[82] M.G. Deceglie, V.E. Ferry, A.P. Alivisatos, and H.A. Atwater, Design of nanostructured solar cells using coupled optical and electrical modeling, *NanoLett.* **12**, 2894-2900 (2012).

[83] S. Pillai, K.R. Catchpole, T. Trupke, and M.A. Green, Surface-plasmon enhanced silicon solar cells, *J. Appl. Phys.* ***101***, 093105 (2007).

[84] K.R. Catchpole and A. Polman, Plasmonic solar cells, *Optics Express* **16**, 21793-21800 (2008).

[85] V.E. Ferry, L.A. Sweatlock, D. Pacifici, and H.A. Atwater, Plasmonic nanostructure design for efficient light coupling into solar cells, *NanoLett.* **8**, 4391-4397 (2008).

[86] Yu.A. Akimov, K. Ostrikov, and E.P. Li, Surface plasmon enhancement of optical absorption in thin-film silicon solar cells, *Plasmonics* **4**, 107-113 (2009).

[87] H. Tan, R. Santbergen, A.H.M. Smets, and M. Zeman, Plasmonic light trapping in thin-film silicon solar cells with improved self-assembled silver nanoparticles, *NanoLetters* **12**, 4070-4076 (2012).

[88] F. J. Beck, A. Polman, and K. R. Catchpole, Tunable light trapping for solar cells using localized surface plasmons, *J. Appl. Phys.* **105**, 114310 (2009).

[89] H.-M. Li, G. Zhang, C. Yang, D.-Y. Lee, Y.-D. Lim, T.-Z. Shen, W.J. Yoo, Y.J. Park, H. Kim, S.N. Cha, and J. M. Kim, Enhancement of light absorption using high-k dielectric in localized surface plasmon resonance for silicon-based thin film solar cells, *J. Applied Physics* **109**, 093516 (2011).

[90] A. Tamang, H. Sai, V. Jovanov, M.I. Hossain, K. Matsubara, and D. Knipp, On the interplay of cell thickness and optimum period of silicon thin-film solar cells: light trapping and plasmonic losses, *Prog. Photovolt: Res. Appl.* **24**, 379–388, (2016).

[91] P.H. Wang, M. Theuring, M. Vehse, V. Steenhoff, C. Agert, and A.G. Brolo, Light trapping in a-Si:H thin-film solar cells using silver nanostructures, *AIP Advances* **7**, 015019 (2017).

[92] K. Domanski, J. Correa-Baena, N. Mine, M. Nazeeruddin, A. Abate, M. Saliba, W. Tress, A. Hagfeldt, and M. Grätzel, Not all that glitters is gold: metal-migration-induced degradation in perovskite solar cells, *ACS Nano* **10**, 6306-6314 (2016).

[93] R.A. Pala, J. White, E. Barnard, J. Liu, and M.L. Brongersma, Design of plasmonic thin-film solar cells with broadband absorption enhancements, *Advanced Materials* **21**, 1-6 (2009).

[94] W. Wang, S. Wu, K. Reinhardt, Y. Lu, and S. Chen, Broadband light absorption enhancement in thin-film silicon solar cells, *NanoLetters* **10**, 2012–2018 (2010).

[95] M. Omelyanovich, Y. Ra'di and C. Simovski, Perfect plasmonic absorbers for photovoltaic applications, *J. Optics* **17**, 125901 (2015).

[96] C. Simovski, *Thin-film photovoltaic cell structure, nanoantenna and method for manufacturing.* US Patent No 9252303 B2, issued on Feb. 2, 2016.

[97] C. Simovski, D. Morits, P. Voroshilov, P. Belov, M. Guzhva, and Yu. Kivshar, Enhanced efficiency of light-trapping nanoantenna arrays for thin-film solar cells, *Optics Express* **21**, A714–A725 (2013).

[98] P.M. Voroshilov, C.R. Simovski, and P.A. Belov, Nanoantennas for enhanced light trapping in transparent organic solar cells, *J. Mod. Optics* **61**, 1743-1748 (2014).

[99] P. Voroshilov, V. Ovchinnikov, A. Papadimitratos, A. Zakhidov, and C. Simovski, Light trapping enhancement by silver nanoantennas in organic solar cells, *ACS Photonics 5*, 1767-1772 (2018).

[100] P.M. Voroshilov and C.R. Simovski, Leaky domino-modes in regular arrays of substantially thick metal nanostrips, *Phot. Nanostruct. Fund. Applic.* **20**, 18-30 (2016).

[101] J.N. Munday and H.A. Atwater, Large integrated absorption enhancement in plasmonic solar cells by combining metallic gratings and antireflection coatings, *NanoLetters* **10**, 2195-2201 (2010).

[102] C. Li, L. Xia, H. Gao, R. Shi, C. Sun, H. Shi, and C. Du, Broadband absorption enhancement in a-Si:H thin-film solar cells sandwiched by pyramidal nanostructured arrays, *Optics Express* **20**, A589–A595 (2012).

[103] P. Spinelli and A. Polman, Prospects of near-field plasmonic absorption enhancement in semiconductor materials using embedded Ag nanoparticles, *Opt. Express* **20**, A641-A654 (2012).

[104] V.E. Ferry, M.A. Verschuuren, H.B.T. Li, E. Verhagen, R.J. Walters, R.E.I. Schropp, H.A. Atwater and A. Polman, Light trapping in ultrathin plasmonic solar cells, *J. Opt.* **14**, 024002 (2012).

[105] J. Grandidier, R.A. Weitekamp, M.G. Deceglie, D.M. Callahan, C. Battaglia, C.R. Bukowsky, C. Ballif, R.H. Grubbs, and H.A. Atwater, Solar cell efficiency enhancement via light trapping in printable resonant dielectric nanosphere arrays, *Physica Status Solidi A* **210**, 255-260 (2012).

[106] C.R. Simovski, A.S. Shalin, P.M. Voroshilov, and P.A. Belov, Photovoltaic absorption enhancement in thin-film solar cells by non-resonant beam collimation by submicron dielectric particles, *J. Appl. Phys.* **114**, 103104 (2013).

[107] M. Omelyanovich, V. Ovchinnikov, and C. Simovski, A non-resonant dielectric metamaterial for enhancement of thin-film solar cells, *J. Optics* **17**, 025102 (2015).

[108] A. Heifetz, S.-C. Kong, A.V. Sahakian, A. Taflove, and V. Backman, Photonic nanojets, *J. Comput. Theor. Nanosci.* **6**, 1979–1992 (2009).

[109] N. Horriuchi, Photonic nanojets, *Nature Phot.* **6**, 138–139 (2012).

[110] D. McCloskey, K.E. Ballantine, P.R. Eastham, and J.F. Donegan, Photonic nanojets in Fresnel zone scattering from non-spherical dielectric particles, *Opt. Express* **20**, 128–140 (2012).

[111] A. Neves, Photonic nanojets in optcal tweezers, *J. Qunatitative Spectroscopy and Radiative Transfer* **162**, 122-132 (2015).

[112] S. Yang, F. Wang, Y. Ye, Y. Xia, Y. Deng, J. Wang, and Y. Cao, Influence of the photonic nanojet of microspheres on microsphere imaging, *Opt. Express* **25**, 27551-27558 (2017).

[113] J.Y. Chen and K.W. Sun, Enhancement of the light conversion efficiency of silicon solar cells by using nanoimprint anti-reflection layer, *Solar Energy Mater. Solar Cells* **94**, 629-639 (2010).

[114] D.A.Baranov, P.A.Dmitriev, I.S.Mukhin, A.K.Samusev, P.A.Belov, C.R.Simovski, and A.S.Shalin, Broadband antireflective coatings based on two-dimensional arrays of subwavelength nanopores, *Appl. Phys. Lett.* **106**, 171913 (2015).

[115] P. M. Voroshilov, C.R. Simovski, P.A. Belov, and A.S. Shalin, Light-trapping and antireflective coatings for amorphous Si-based thin-film solar cells, *J. Appl. Phys.* **117**, 203101 (2015).

[116] M.M. Omelyanovich and C.R. Simovski, Wide-angle light-trapping electrode for photovoltaic cells, *Opt. Letters* **42**, 3726-3729 (2017).

[117] Y. Wang, X. Zhang, B. Han, L. Bai, H. Zhao, F. Yang, J. Liang, Q. Huang, X. Chen and Y. Zhang, UV micro-imprint patterning for tunable light trapping in p-i-n thin-film silicon solar cells *Appl. Surf. Sci.* **355**, 14-18 (2015).

[118] C.S. Schuster, S. Morawiec, M. J. Mendes, M. Patrini, E.R. Martins, L. Lewis, I. Crupi, And T.F. Krauss, Plasmonic and diffractive nanostructures for light trapping—an experimental comparison, *Optica* **2**, 194-200 (2015).

[119] P.M. Voroshilov and C.R. Simovski, Affordable universal light-trapping structure for third-generation photovoltaic cells, *JOSA B* **34**, D77 (2017).

[120] C. Zhang, Y. Song, M. Wang, M. Yin, X. Zhu, L. Tian, H. Wang, X. Chen, Z. Fan, L. Lu, and D. Li, Efficient and flexible thin film amorphous silicon solar cells on nanotextured polymer substrate using sol–gel based nanoimprinting method, *Advanced Functional Materials* **27**, 1604720 (2017).

Index